

# Gap Flows Along the Columbia River Observed During the WFIP2 Field Campaign

---

Environmental Science Division

### **About Argonne National Laboratory**

Argonne is a U.S. Department of Energy laboratory managed by UChicago Argonne, LLC under contract DE-AC02-06CH11357. The Laboratory's main facility is outside Chicago, at 9700 South Cass Avenue, Lemont, Illinois 60439. For information about Argonne and its pioneering science and technology programs, see [www.anl.gov](http://www.anl.gov).

### **DOCUMENT AVAILABILITY**

**Online Access:** U.S. Department of Energy (DOE) reports produced after 1991 and a growing number of pre-1991 documents are available free at OSTI.GOV (<http://www.osti.gov/>), a service of the US Dept. of Energy's Office of Scientific and Technical Information.

### **Reports not in digital format may be purchased by the public from the National Technical Information Service (NTIS):**

U.S. Department of Commerce  
National Technical Information Service  
5301 Shawnee Rd  
Alexandria, VA 22312  
**[www.ntis.gov](http://www.ntis.gov)**  
Phone: (800) 553-NTIS (6847) or (703) 605-6000  
Fax: (703) 605-6900  
Email: [orders@ntis.gov](mailto:orders@ntis.gov)

### **Reports not in digital format are available to DOE and DOE contractors from the Office of Scientific and Technical Information (OSTI):**

U.S. Department of Energy  
Office of Scientific and Technical Information  
P.O. Box 62  
Oak Ridge, TN 37831-0062  
**[www.osti.gov](http://www.osti.gov)**  
Phone: (865) 576-8401  
Fax: (865) 576-5728  
Email: [reports@osti.gov](mailto:reports@osti.gov)

### **Disclaimer**

This report was prepared as an account of work sponsored by an agency of the United States Government. Neither the United States Government nor any agency thereof, nor UChicago Argonne, LLC, nor any of their employees or officers, makes any warranty, express or implied, or assumes any legal liability or responsibility for the accuracy, completeness, or usefulness of any information, apparatus, product, or process disclosed, or represents that its use would not infringe privately owned rights. Reference herein to any specific commercial product, process, or service by trade name, trademark, manufacturer, or otherwise, does not necessarily constitute or imply its endorsement, recommendation, or favoring by the United States Government or any agency thereof. The views and opinions of document authors expressed herein do not necessarily state or reflect those of the United States Government or any agency thereof, Argonne National Laboratory, or UChicago Argonne, LLC.

# Gap Flows Along the Columbia River Observed During the WFIP2 Field Campaign

---

prepared by

Virendra P. Ghaté<sup>1</sup>, Joseph B. Olson<sup>2</sup>, Katherine E. Szoldatits<sup>1</sup>, and David D. Turner<sup>2</sup>

1. Environmental Science Division, Argonne National Laboratory.

2. NOAA Global Systems Laboratory.

02-01-2022

## CONTENTS

ACKNOWLEDGMENTS .....	vi
ABSTRACT .....	1
1 INTRODUCTION .....	1
2 DATA AND INSTRUMENTATION.....	3
3 IDENTIFICATION AND LARGE-SCALE CONDITIONS DURING GAP FLOW EVENTS .....	6
4 RELATIONSHIP BETWEEN ZONAL WIND SPEED AND ZONAL PRESSURE GRADIENT .....	11
4.1 Daily Timescales.....	11
4.1.1 Wasco.....	11
4.1.2 Troutdale.....	13
4.1.3 Boardman.....	15
4.2 Diurnal Timescales .....	18
4.2.1 Wasco.....	18
4.2.2 Boardman.....	20
5 PERFORMANCE OF THE HRRR MODEL.....	22
6 SUMMARY AND DISCUSSION.....	27
REFERENCES .....	29

## FIGURES

1 Latitude-longitude maps of the terrain height above mean sea level at 30 m resolution, at 750 m resolution, and at 3 km resolution of the study region .....	3
2 Profile of daily average wind speed at Wasco during August 2016.....	7
3 Number of local days as a function of months during the WFIP2 field campaign at Troutdale, Wasco, and Boardman .....	8
4 <i>Top:</i> Latitude-longitude maps of 2 m potential temperature, surface air pressure, and winds during locally forced westerly wind days and locally forced easterly wind days identified at Wasco. <i>Middle:</i> Average change in 2 m potential temperature from the climatological mean during local westerly days and local easterly days. <i>Bottom:</i> Average difference in surface air pressure from the climatological mean during locally forced westerly days and locally forced easterly days.....	10
5 Scatter plots of observed pressure differences at the surface between the Troutdale and Boardman sites and 200 m zonal wind speed at Wasco.....	12
6 Averaged observed vertical profiles of zonal and meridional wind speeds for easterly local days and westerly local days at Wasco for different surface pressure differences between Troutdale and Boardman.....	13

## FIGURES (CONT.)

7	Scatter plots of observed pressure differences at the surface between Troutdale and Boardman sites and 200 m zonal wind speed at Troutdale .....	14
8	Averaged observed vertical profiles of zonal and meridional wind speeds for easterly local days and westerly local days at Troutdale for different surface pressure differences between Troutdale and Boardman. ....	15
9	Scatter plots of pressure difference at the surface between Troutdale and Umatilla sites and 200 m zonal wind speed at Boardman .....	16
10	Averaged vertical profiles of zonal and meridional RWP wind speeds for easterly local days and westerly local days at Boardman for different pressure differences between Troutdale and Umatilla.....	17
11	Average diurnal cycles of zonal wind speed during locally forced easterly days at Wasco; local westerly days at Wasco; local easterly days at Wasco with daily averages removed; and local westerly days at Wasco with daily averages removed. ....	19
12	Average diurnal cycles of local zonal pressure gradient and 200 m zonal wind speed at Wasco during westerly days; and scatter plot between the average 200 m zonal wind speed and local zonal pressure gradient at Wasco during westerly gap flow days. ...	20
13	Average diurnal cycles of zonal wind speed during locally forced days at Boardman; local easterly days at Boardman; local westerly days at Boardman; their differences.....	21
14	<i>Top:</i> Average diurnal cycle of the 200 m zonal wind speed and difference between surface air pressure at Troutdale and Umatilla during westerly gap flow days. <i>Bottom:</i> Scatter plot between the 200 m zonal wind speed at Boardman, and pressure differences between Troutdale and Umatilla .....	22
15	Scatter plots of daily averaged pressure differences between Troutdale and Boardman and 200 m zonal wind speed; during local days at Wasco from observations simulated by HRRR-3km and by HRRR-750m; between observed and HRRR model-simulated pressure differences between Troutdale and Boardman during local days; and between observed and HRRR-simulated 200 m zonal wind speed at Wasco during local days. ....	23
16	Zonal and meridional wind speeds as observed and simulated with the HRRR-3km and HRRR-750m models for local westerly and local easterly days with pressure differences between Troutdale and Boardman of 7–17 hPa.....	25
17	For the locally forced westerly days, box plots showing the diurnal cycle of surface air pressure at Troutdale, surface air pressure at Boardman, the difference between surface air pressure at Troutdale and Boardman, and the 200 m zonal wind speed.....	26
18	Phase diagram between the zonal pressure gradient and the 200 m zonal wind speeds at Wasco during locally forced westerly gap flow days as observed and as simulated by the HRRR model at 750 m spatial resolution. ....	27

## TABLE

1	Available measurement or output of the datasets and their characteristics.....	4
---	--	---

## ACKNOWLEDGMENTS

VG would like to acknowledge funding from the U.S. Department of Energy's Energy Efficiency Renewable Energy Wind Energy Technology Office. This work was also supported by the National Oceanic and Atmospheric Administration Atmospheric Science for Renewable Energy program. We would also like to thank numerous site personnel involved in the WFIP2 project. We gratefully acknowledge the computing resources provided on Bebop, a high-performance computing cluster operated by the Laboratory Computing Resource Center at Argonne National Laboratory.



# **GAP FLOWS ALONG THE COLUMBIA RIVER OBSERVED DURING THE WFIP2 FIELD CAMPAIGN**

## **ABSTRACT**

Data collected in the Columbia River Gorge and Basin Area during the second Wind Forecasting Improvement Project (WFIP2) was used to study gap flow events in the region. In particular, the relationship between 200 m zonal wind speed and the zonal mesoscale pressure gradient at Troutdale (West of the gorge), Wasco (east of the gorge), and Boardman (farther east of the gorge) sites was examined. An objective criterion was used to identify 169 (Troutdale), 161 (Wasco), and 113 (Boardman) gap flow days that had weak synoptic forcing. The 200 m zonal wind speed exhibited a linear relationship with the zonal pressure gradient at Wasco during both easterly and westerly gap flow days at daily timescales. Such a relationship was only observed during easterly gap flow days at Troutdale and was not observed at Boardman. The zonal wind speed exhibited a diurnal cycle at Wasco and Boardman, with greater changes in the nighttime winds than the daytime winds due to changes in pressure gradient. The root mean square differences (RMSDs) between the observed pressure gradient at Wasco and that simulated by the High Resolution Rapid Refresh (HRRR) model in 3 km (HRRR-3km) and 750 m (HRRR-750m) horizontal resolution were 3.14 hPa and 0.57 hPa, respectively. However, the RMSDs for the 200 m zonal wind speed were  $1.40 \text{ m s}^{-1}$  for HRRR-3km and  $1.20 \text{ m s}^{-1}$  for HRRR-750m. Improvement in simulating the zonal pressure gradient accompanied by negligible changes in simulating zonal wind speed due to higher horizontal resolution points to a complex interplay between different components of the model physics when simulating the meteorology. The HRRR-750m resolution model accurately mimicked the observed covariability (phase diagram) between the zonal pressure gradient and the 200 m zonal wind speed during the nighttime, but not during the daytime, suggesting model errors might be related to the representation of boundary layer processes.

## **1 INTRODUCTION**

The Cascade mountains are oriented north-south about 250 km inland from the Pacific coast and spanning the U.S. states of Washington and Oregon. The mountain range, with peak heights exceeding 3 km, acts as a barrier between the western marine climate regime and the more arid terrain-forced climate regime to the east. The local weather and meteorology of the region is complicated by the presence of the Columbia River Gorge, which cuts through the Cascades and the Columbia Basin from east to west.

This complex topography generates different weather phenomena, such as cold pools (Adler et al. 2021; Arthur et al. 2021), gap flows (Banta et al. 2021), mountain waves (Draxl et al. 2021), marine air intrusions (Banta et al. 2020), and wakes that affect the local weather. Cold pools in the region are known to stratify the atmosphere, thereby trapping the pollutants and causing

freezing rain (Whiteman et al. 2001, Steenburgh et al. 1997, Zhong et al. 2001, McCaffrey et al., 2019). The cold pools have been shown to be associated with weak mid-level synoptic scale flow in the region (Reeves and Stensrud 2009).

Gap flows result from a zonal pressure gradient in the region, often producing very high winds and extreme precipitation (Sharp and Mass 2002, Sharp and Mass 2004). During the summer months a climatological high-pressure over the North Pacific and low pressure over the Columbia River Basin results in frequent westerly gap flows, while easterly gap flows nominally occur during the winter months due to higher pressure and colder temperatures inland compared with over the Pacific. Both the easterly and westerly gap flows can result in high-wind conditions in the towns along the Columbia River, with the magnitude of the winds modulated by the Columbia River Gorge and the zonal pressure gradient. The easterly gap flows are known to interact with synoptic scale systems resulting in extreme weather and precipitation (Wantz and Sinclair 1981, Colle and Mass 2000, Neiman et al. 2018).

The region is also home to many wind farms, which together produce more than 6 GW of energy (Wilczak et al. 2019). Accurate forecasts of wind power can reduce the cost of wind energy (Marquis et al. 2011) and accelerate expansion of wind energy. Forecasting wind power requires accurate predictions at high (e.g., 15 minute) temporal resolution of wind speed and direction and their variations with height (shear and veer) in the lowest 200 m. Forecasting winds in this region is challenging due to the local weather phenomena mentioned above and the interactions among them (Pichugina et al. 2019, Pichugina et al. 2020, Bianco et al. 2021). Brewer and Mass (2014) have shown that the Weather Research and Forecasting (WRF) model, using 1,300 m horizontal grid spacing and initialized using reanalysis datasets (Kalnay et al., 1996), is capable of simulating the dominant local meteorology of the region; however, the model's ability to forecast turbine-level winds during gap flow events has not been tested. Olson et al. (2019) and Bianco et al. (2019) showed a considerable improvement in the forecast of hub height winds with reductions in the model grid spacing from 3 km to 750 m; however, even at 750 m several terrain features in the region remain unresolved (Figure 1).

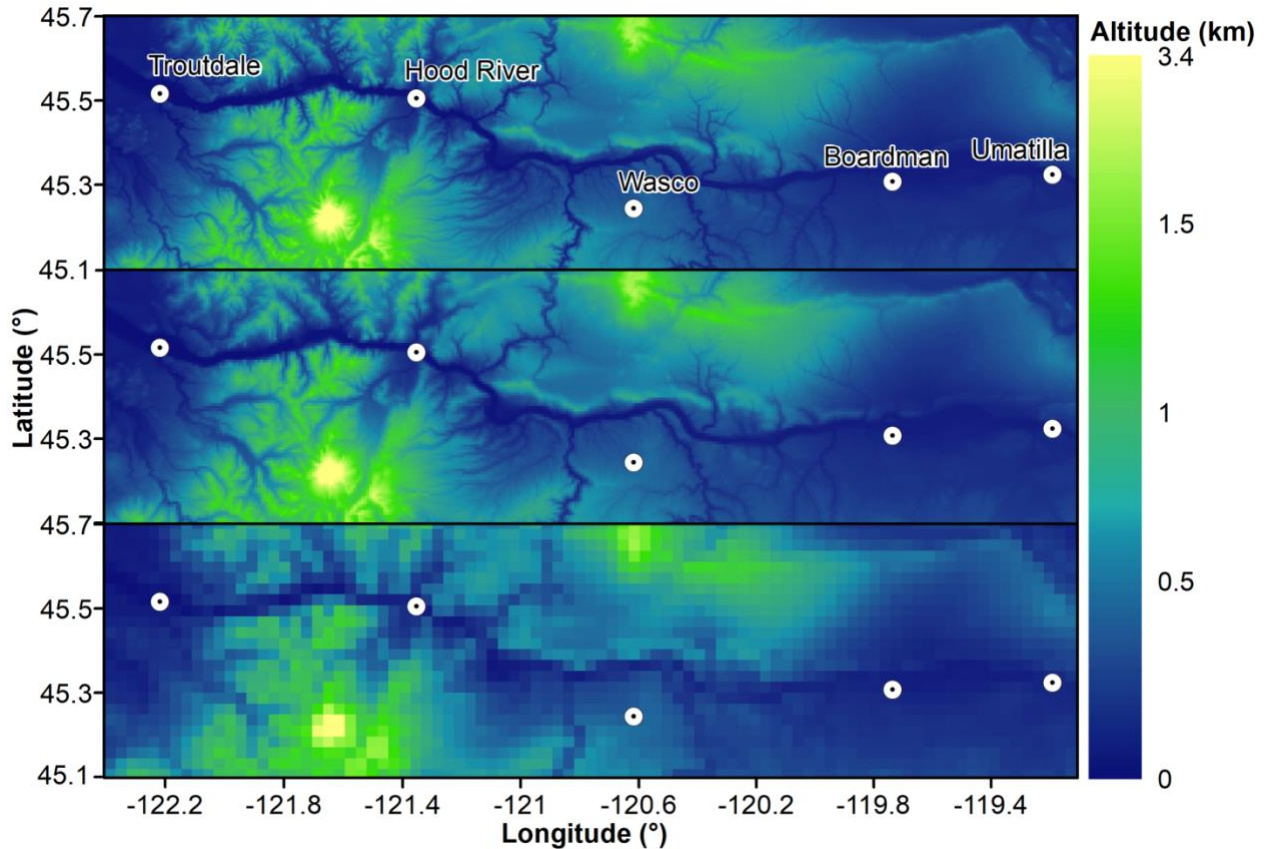


**FIGURE 1** Latitude-longitude map of the terrain height above mean sea level at 30 m resolution (*top*), at 750 m resolution (*middle*), and at 3 km resolution (*bottom*) of the study region with locations of the sites from which the data was collected indicated by the white circles.

In this study we use observations made at five sites along the Columbia River during the Second Wind Forecasting Improvement Project (WFIP2; Shaw et al. 2019) to study gap flow events, particularly the performance of the WRF-based HRRR model (Olson et al. 2019). The specific objectives of this study were (i) to assess the efficacy of the zonal (east-west) pressure gradient in determining low-level zonal winds during gap flow events, and (ii) to evaluate the performance of a numerical weather prediction model in forecasting winds during these days. We focused on gap flow events that were forced by local weather and had weaker synoptic forcing because model errors were relatively easy to identify for these events compared with events strongly forced by synoptic weather.

## 2 DATA AND INSTRUMENTATION

In this study we used data collected during WFIP2. Multiple instruments at many sites were deployed from October 2015 to April 2017 in the U.S. states of Washington and Oregon as a part of WFIP2 (Wilczak et al. 2019). From the arrays of instrumentation, we used data collected at five sites that lie along the Columbia River roughly in a westerly direction: Troutdale, Hood River, Wasco, Boardman, and Umatilla. The complete set of instrumentation and their operation was reported in Wilczak et al. (2019), and the model configuration was described in Olson et al. (2019).

The variables, spatial and temporal resolution, and data availability from the instruments and the model simulations are reported in Table 1.

**TABLE 1: Available measurement or output of the datasets and their characteristics.**

Instrument/Model Name	Measurement/Output	Resolution	Data Availability (no. of days out of total 548)
Surface meteorological instrument (MET)	Temperature, water vapor mixing ratio, pressure, and winds	1–2 minutes	Troutdale: 535 Hood River: 504 Wasco: 546 Boardman: 548 Umatilla: 473
Microbarograph	Surface air pressure	20 Hz	Troutdale: 398 Hood River: 404 Wasco: 471 Boardman: 407 Umatilla: 405
Radar Wind Profiler (RWP)	Profiles of zonal and meridional wind components	Hourly profiles at 58 m resolution from 138 m to 2.51 km for low-power mode, and 102 m resolution from 145 m to 6.02 km for high-power mode	Troutdale: 547 Wasco: 544 Boardman: 464
Sound Detection and Ranging (SODAR)	Profiles of zonal and meridional wind components	15 minute profiles at 10 m range resolution from 30 m to 200 m	Troutdale: 0 Wasco: 548 Boardman: 533
HRRR model output	Surface temperature, pressure, humidity, winds, sensible and latent heat fluxes, and friction velocity; profiles of temperature, humidity, pressure, and winds	15 minute values every 20–200 m from surface to 5 km for 3 km and 750 m horizontal resolution	Troutdale: 219 Wasco: 219 Boardman: 219

The radar wind profilers (RWP) operated at 915 MHz and recorded the full Doppler spectrum and its moments at 30 second temporal resolution and 97 m and 57 m range resolution for the low-resolution and high-resolution modes, respectively. The lowest- and highest-range gates of the low-resolution modes were 187 m and 6,023 m, respectively, and for the high-resolution modes were 81 m and 2,542 m, respectively. Consensus winds were calculated from the moments data at an hourly temporal resolution for both modes. The Sound Detection and Ranging (SODARs) reported the wind profiles with a 10 m range resolution every 15 minutes from 30–200 m above the ground. A meteorological station was also present at all sites, recording the surface air temperature, relative humidity, pressure, and winds at 1–2 minute temporal resolution. There were some small differences in the range and temporal resolutions of the instruments across the

sites that we have not described. High-precision barometers combined with Nishiyama-Bedard quad disk pressure probes (Nishiyama and Bedard 1991), here referred to as microbarographs, measured pressure at the surface, nominally 2 m above ground level at a 20 Hz temporal resolution. Due to their better resolution (0.0001%), accuracy ( $\pm 0.08$  hPa), and stability (better than 0.1 hPa per year) compared with the meteorological station barometers, the data from the microbarographs was used for deducing mesoscale pressure gradients.

Simulations of the HRRR model were made in a reforecast mode for four six-week periods over the entire domain (Olson et al. 2019; Benjamin et al. 2016). The output from these model simulations over three of the sites that contained RWP were extracted. Near-surface meteorological variables such as winds and fluxes, along with profiles of winds, temperature, humidity, and pressure from grid cells closest to the site, were extracted at a 15 minute temporal resolution. The model simulations were made at both 750 m and 3 km horizontal grid spacing using both the control configuration (which was the state of the HRRR prior to WFIP2) and an experimental configuration that included a new set of parameterizations derived as part of the WFIP2 analysis (Olson et al. 2019). The 200 m zonal wind speeds and the zonal pressure gradients (discussed later) were similar in simulations made with the control and experimental setup. Hence, in this study we used output from simulations made in the control setup at both 3 km and 750 m horizontal grid spacing. The model data was interpolated to a resolution of 20 m from the surface to 200 m, 50 m from 200 to 500 m, 100 m from 500 m to 2 km, and 200 m from 2 km to 5 km. We elected to only use HRRR output for forecast hours 12 through 24 to avoid complications associated with model spin-up. The HRRR model output at the grid point closest to the sites at Troutdale, Wasco, and Boardman were available on about 219 days of the field campaign.

Observation sites at Troutdale, Wasco, and Boardman were at 21 m, 423 m, and 100 m above the mean sea level. The closest model grid point for the 3 km (750 m) model domain was 1,394 (316) m, 1,654 (353) m and 1,679 (298) m away from the observation site at Troutdale, Wasco, and Boardman, respectively. The elevations above mean sea level of the closest model grid point for the 3 km (750 m) resolution model simulation were 21 (17) m, 423 (450) m, and 100 (121) m at Troutdale, Wasco, and Boardman, respectively. The greatest changes in elevation in any direction at Troutdale, Wasco, and Boardman deduced from adjacent grid-points in the 30 m resolution elevation data were 0.6%, 1.7%, and 1.9%, respectively, while the same at 750 m (3 km) were 0.1% (0.4%), 1.4% (1.5%), and 1.2% (0.8%), respectively. Hence, a model grid cell too far away would have rendered atmospheric properties at a different terrain elevation, especially the surface air pressure that was used to calculate mesoscale pressure gradient, thereby hindering model evaluation. However, for both resolutions of the HRRR the elevation at the closest grid cell was only a few tens of meters different than the observed, while between the two HRRR versions the differences were even smaller, thus enabling model evaluation. The average differences between the observed and HRRR-3km (HRRR-750m) simulated surface air pressure at Troutdale, Wasco, and Boardman were 0.32 (-0.23) hPa, 4.71 (1.64) hPa, and 2.60 (0.23) hPa, respectively. The average differences between the surface air pressure at Troutdale and Boardman as observed and simulated by HRRR-3km (HRRR-750m) were 13.05 hPa and 10.14 (12.96) hPa, respectively.

To account for differences in the sampling volumes and temporal resolutions of the instruments and the model output, all of the variables were averaged to a uniform hourly temporal resolution from October 1, 2015, to April 1, 2017 (548 days). The wind profiles from the low- and high-power RWP modes were interpolated and averaged to a uniform 50 m vertical resolution from 200 m to 6 km at hourly timescales. These profiles were further merged with the SODAR winds to generate wind profiles from 30 m to 6 km with a resolution of 10 m from 30 m to 200 m and 50 m from 200 m to 6 km. Due to the differences in the operational characteristics of the SODAR and RWP, there were some discontinuities in the generated wind profiles between 150 m and 200 m. Wind profiles reported from the RWP low-power mode, RWP high-power mode, SODAR, and the calculated merged profiles for August 2016 are shown in the supplemental material as an example. For the entire campaign, 3,153 hours (24%) of the merged wind profiles had a gap in them due to the highest height of SODAR reported winds being lower than the first usable range gate of the RWP low-power mode. The difference between the SODAR-reported hourly wind speed and that from the RWP low-power mode was within  $1 \text{ m s}^{-1}$  for 62% and less than  $2 \text{ m s}^{-1}$  for 79%. It is beyond the scope of this study to probe the reasoning behind these differences or study their variability with atmospheric conditions.

### 3 IDENTIFICATION OF GAP FLOW EVENTS

The study area is often influenced by synoptic-scale weather phenomena, so it was essential to identify gap flow days that had minimal synoptic-scale influence with meteorological conditions mostly forced by processes acting at meso- $\alpha$  (200 km) or finer spatial scales. From the event log (<https://a2e.energy.gov/data/wfip2/log.z01.00>) maintained by WFIP2 investigators during the field study, it was deduced that during synoptically forced days the wind speeds increased at all levels from surface to 3 km (above the boundary layer), while during locally forced gap flow days the winds were slower than average above the boundary layer. Similarly, locally forced gap flow days were identified using the following criteria:

$$Wspd_{day} < Wspd_{month} - 0.5 \times Wspd_{std}$$

where  $Wspd_{day}$  is the averaged wind speed at 1.5 km during local day,  $Wspd_{month}$  was the monthly averaged wind speed at 1.5 km, and  $Wspd_{std}$  was the monthly standard deviation of wind speed at 1.5 km. The hourly averaged wind speeds generated from the RWP and SODAR winds were used to generate the daily and monthly averages.

The primary notion behind the identification criteria was that synoptic forcing will tend to increase winds in the lower troposphere through at least several kilometers, while local surface forcing primarily results in enhanced winds confined to the boundary layer. The level of 1.5 km was chosen as it was typically above the boundary layer and observations from the RWP were available at this level for most of the field campaign. During dry wintertime conditions the highest level of reliable observations by the RWP was reduced due to reduction in Bragg scattering, hence the identification criteria couldn't be applied to 30, 41, and 1 day at Wasco, Boardman, and Troutdale, respectively. Because the criteria require wind fields at 1.5 km, they were only applied to sites having the RWP.

The identification criteria were demonstrated using the data collected during August (Figure 2). Local weather observers at the site documented weather events such as gap flows, cold pools, mountain waves, topographic wakes, and convective outflows during this period, with more than one weather event recorded on each day. Cross-barrier flows were identified on 23 days, with 18 days identified as cross-barrier thermal and 22 days identified as cross-barrier synoptic. The monthly average wind speed at 1.5 km in August 2016 was  $6.40 \text{ m s}^{-1}$  with a standard deviation of  $3.94 \text{ m s}^{-1}$ , yielding a threshold of  $4.43 \text{ m s}^{-1}$  for identifying gap flows. Eleven of the 23 days were identified as locally forced gap flow days according to the objective criteria in equation 1. Cross-barrier flow was recorded on over 300 days during the campaign (Wilczak et al. 2019), out of which the objective criteria identified 161 days. A more sophisticated criterion for identifying gap flows that uses zonal pressure gradients along with self-organizing weather maps might yield different results. However, it was beyond the scope of this study to develop such criteria.

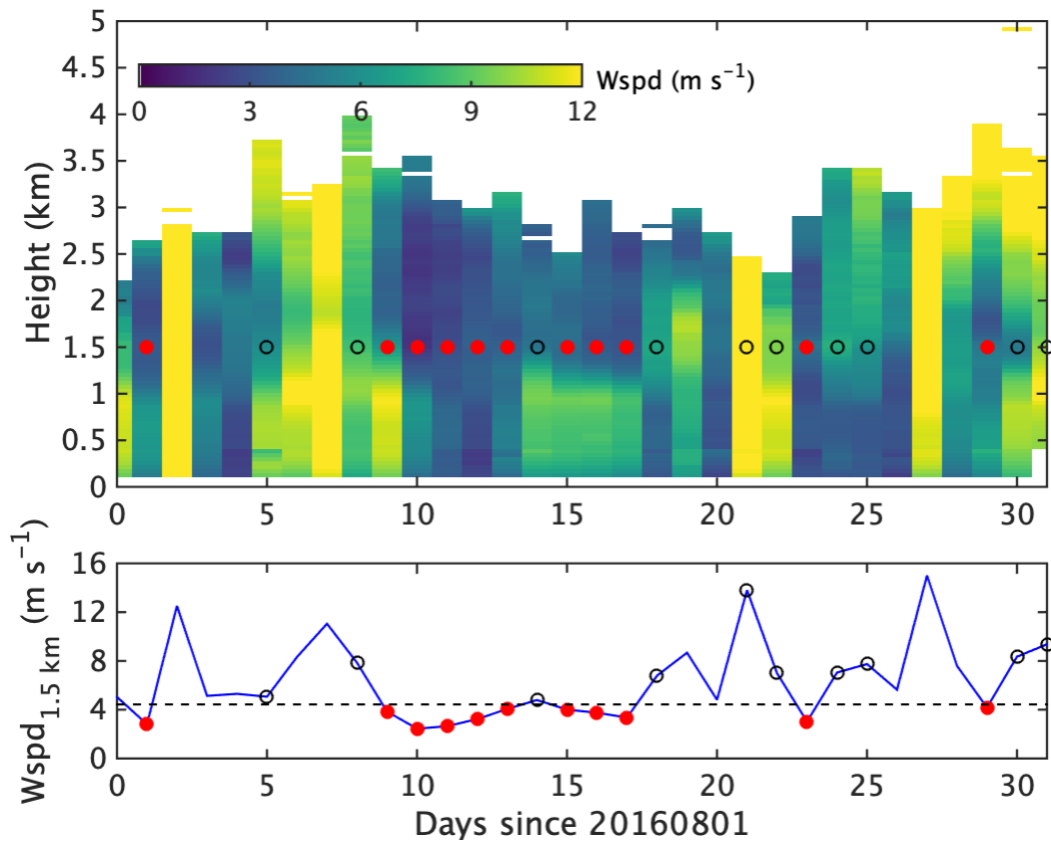


**FIGURE 2** *Top:* Profile of daily average wind speed at Wasco during August 2016. *Bottom:* Daily average wind speed at 1.5 km at Wasco during August 2016. In both panels the black circles denote days that were reported to have gap flow events by the local observers and the red circles denote days identified as having gap flow events from the proposed objective criteria. The dashed black line in the bottom panel is the limit used for identifying locally forced days.

Of the 548 days of the WFIP2 campaign, 169 (31%), 161 (29%), and 113 (21%) days were identified as locally forced at Troutdale, Wasco, and Boardman, respectively. The days identified as having easterly gap flow events (8–9 April) and westerly gap flow events (28–30 June), analyzed further in Wilczak et al. (2019), were accurately identified as locally forced. Approximately 10 days per month were found to be locally forced at each of the three sites, and this number showed little seasonal variation (Figure 3). The locally forced days were further classified using wind direction (Wdir) at 200 m as northerly, easterly, southerly, and westerly with Wdir within 45° of 0°, 90°, 180°, and 270°, respectively. At Troutdale the majority of the locally forced days had easterly winds, with only 7 days having northerly wind conditions. At Wasco, most locally forced days had westerly wind conditions, with only 5 and 3 days having northerly and southerly winds, respectively. Boardman had 65 locally forced days with westerly winds, followed by 27 days with northerly winds and 20 days with easterly winds.

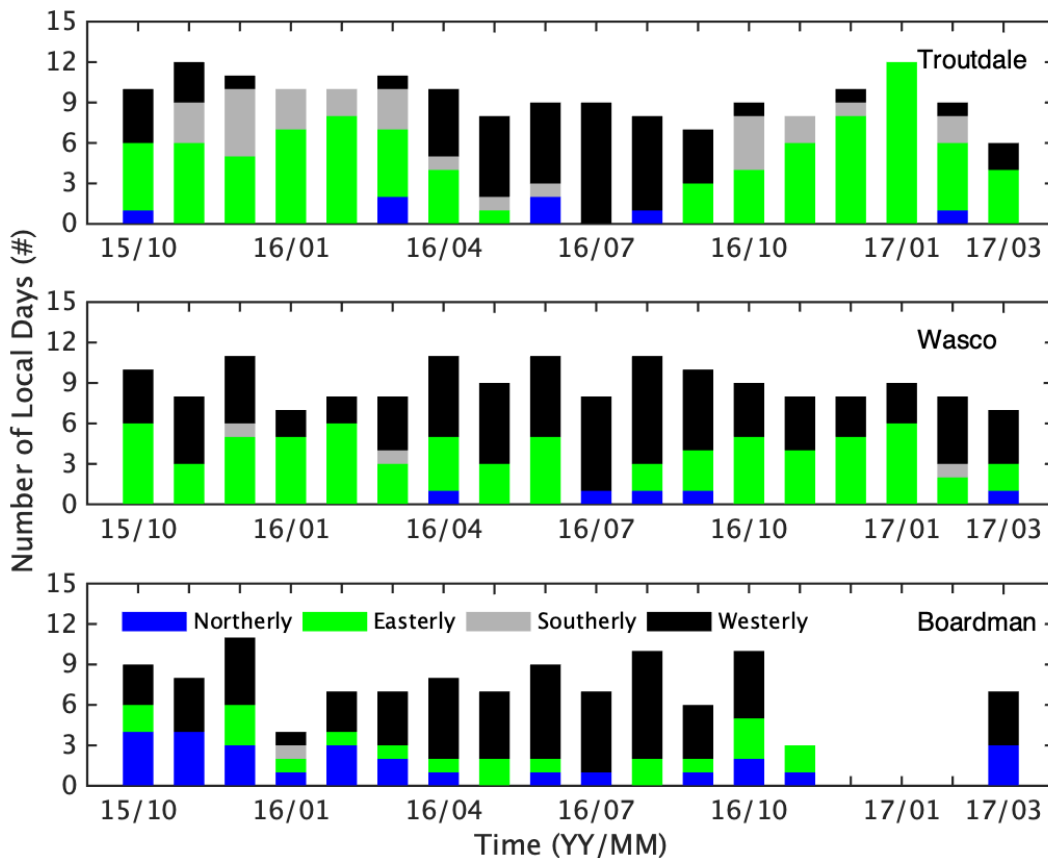


**FIGURE 3** Number of local days as a function of months during the WFIP2 field campaign at Troutdale (*top*), Wasco (*middle*), and Boardman (*bottom*). The bars are color coded by wind direction at 200 m. No data was available at Boardman from 12/2016 to 02/2017. The total length of the bar represents the total number of locally forced days at each location, and the length of each color represents locally forced days with winds from a particular direction.

We identified 26, 30, and 26 days as locally forced days during the summer at Troutdale, Wasco and Boardman, respectively, with 22 (84%), 21 (70%), and 21 (80%) days being local westerly days. For the winter of 2015, we identified 31, 26, and 22 days as locally forced at Troutdale, Wasco, and Boardman, respectively, with winds prevalently from the east at Troutdale (20 days, 64%) and Wasco (16 days, 61%) and from the west at Boardman (9 days, 40%). Collectively, the majority of the locally forced days had winds in the zonal (westerly or easterly) direction at all the three locations, with westerly days dominant in the summer months. To the west of the Cascade Mountains in Troutdale the winds were rarely from the north, while to the east of the Cascade Mountains in Wasco and Boardman the winds were rarely from the south, during locally forced days. This could be due the combined effect of an east-west pressure gradient, the blocking of winds at lower levels by mountains south of Wasco and Boardman, and/or the gentle sloping terrain north of Boardman.

The average potential temperature, pressure, and winds at the surface for the easterly and westerly locally forced days as reported by the North American Regional Reanalysis (NARR) are shown in Figure 4. The pressure contours generally follow the terrain, with surface pressure of 1,000 hPa over the ocean and at Troutdale, about 980 hPa in the Columbia River Basin, and lower than 900 hPa in the mountains south and north of the study area. The differences in the potential temperature and air pressure from the climatological mean during locally forced easterly and westerly days show higher than average temperature and lower than average pressure in the upwind region. It should be noted that changes in surface air temperature at Boardman were around  $\pm 5$  K, while those at Troutdale were around  $\pm 1$  K. The magnitude of the differences in surface air pressure were greater for easterly locally forced days than westerly. The surface air pressure was higher than the climatological mean upwind and similar to the climatological value downwind for both easterly and westerly flows. The changes in the surface air temperature and pressure were consistent with the previous study of Sharp and Mass (2004), suggesting a local circulation in the area. Plots similar to Figure 3 made for local easterly and westerly flow days at Troutdale and Boardman yielded qualitatively similar results.

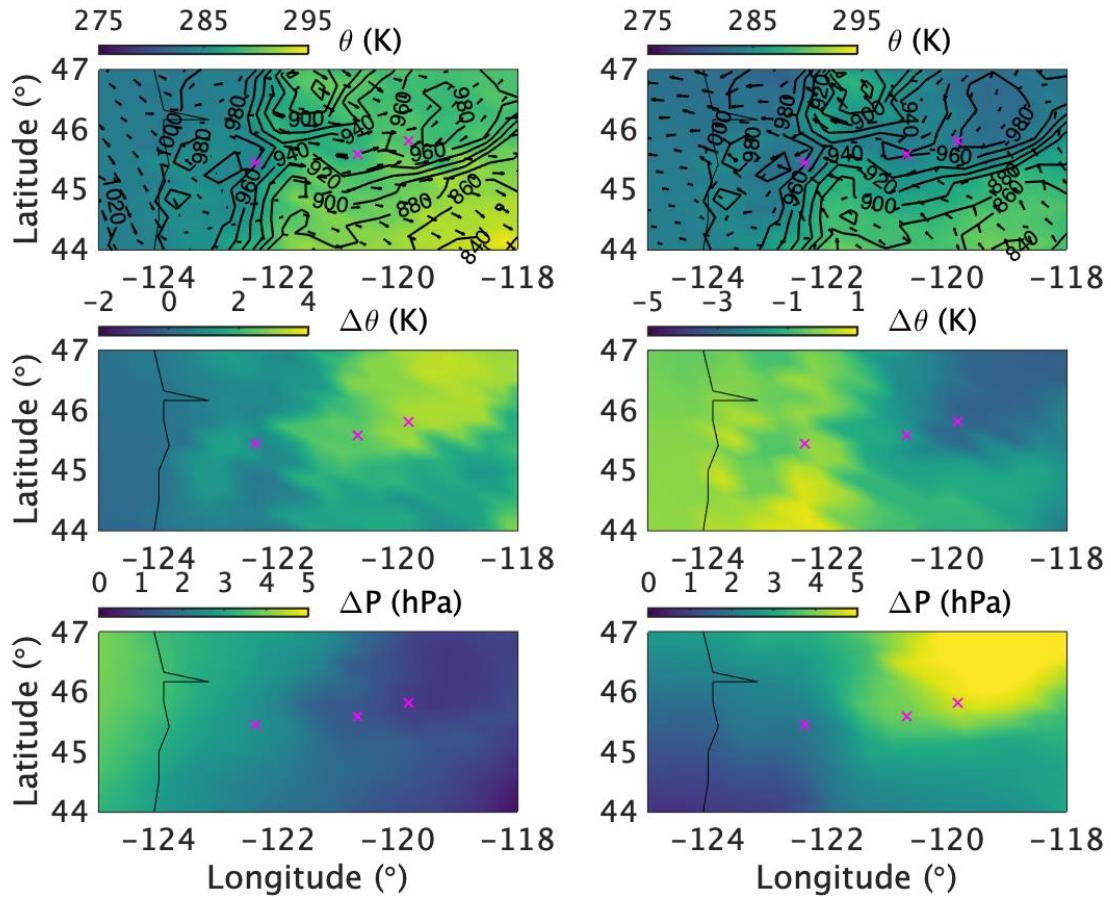


**FIGURE 4** *Top:* Latitude-longitude map of 2 m potential temperature (*shaded colors*), surface air pressure (*contours*), and winds (*arrows*) during locally forced westerly wind days (*left*) and locally forced easterly wind days (*right*) identified at Wasco. *Middle:* Average change in 2 m potential temperature from the climatological mean during local westerly days (*left*), and local easterly days (*right*). *Bottom:* Average difference in surface air pressure from the climatological mean during locally forced westerly days (*left*) and locally forced easterly days (*right*). Troutdale, Wasco, and Boardman are shown in magenta crosses. Output from the NARR model were used for these plots.

## 4 RELATIONSHIPS BETWEEN ZONAL WIND SPEED AND ZONAL PRESSURE GRADIENT

The relationships between the zonal wind speed and the zonal pressure gradient at Troutdale, Wasco, and Boardman were examined next at daily and hourly averaged timescales. Data collected during the locally forced gap flow days was used for the analyses below.

### 4.1 DAILY TIMESCALES

#### 4.1.1 Wasco

A scatter plot of observed pressure differences between Troutdale and Boardman and 200 m zonal wind speeds at Wasco at daily timescales is shown in Figure 5. The pressure differences were calculated from the microbarograph data, and the wind speed from the merged SODAR and RWP data. The average ( $\pm$ standard deviation) pressure difference between Troutdale and Boardman was  $13.05\pm 3.56$  hPa during the study period, and  $15.06\pm 2.12$  hPa and  $9.52\pm 2.34$  hPa, respectively, during locally forced westerly and easterly days. The average 200 m zonal wind speed at Wasco was  $3.48\pm 6.10$  m s<sup>-1</sup>, while during locally forced westerly and easterly flow days it was  $6.73\pm 3.54$  m s<sup>-1</sup> and  $-3.51\pm 2.32$  m s<sup>-1</sup>, respectively. Apart from the local easterly days with pressure differences lower than 6 hPa, the zonal wind speed at 200 m showed a linear relationship with the zonal pressure gradient for both easterly and westerly days. The zonal wind speed strengthened linearly for westerly (easterly) gap flow days with increase (decrease) in the pressure gradient above the mean pressure gradient. The average zonal wind speed was positive (westerly) due to higher number of westerly days. Albeit weak, both easterly and westerly winds existed for pressure differences of 10.4–14.2 hPa.

The locally forced easterly and westerly days at Wasco were further classified based on the pressure differences between Troutdale and Boardman in bins from 2 to 22 hPa every 2 hPa, with a width of 2 hPa. The average profiles of zonal and meridional components of winds at Wasco for different pressure differences between Troutdale and Boardman are shown in Figure 6. The number of samples for locally forced easterly days were 5, 10, 15, and 11 for pressure differences of 6, 8, 10, and 12 hPa, respectively. The number of samples for locally forced westerly days were 11, 17, 26, and 9 for pressure differences of 12, 14, 16, and 18 hPa, respectively. Both easterly and westerly winds occurred for a pressure difference of 12 hPa. A wind jet feature is visible in most of the profiles. Nominally, the nose of the jet was around 400 m. The height of the nose of the jet was different for the zonal and meridional components for most of the days, especially visible for local westerly days with a pressure difference of 18 hPa. An interesting feature was the change in meridional wind from southerly to northerly in the lowest 100 m during local westerly flow days for all pressure difference values. This could be due to frictional turning of part of the Ekman layer during these days, with the flow growing closer to geostrophic balance a few hundred meters above the surface when the pressure gradient was from west to east. For local easterly days, the meridional wind was negligible ( $< 1$  m s<sup>-1</sup>) below 1 km, while local westerly days the meridional component was 30%–50% of the zonal component. Collectively the profiles show the presence of wind shear and veer for all pressure differences, and different heights of wind maxima for zonal and meridional winds.

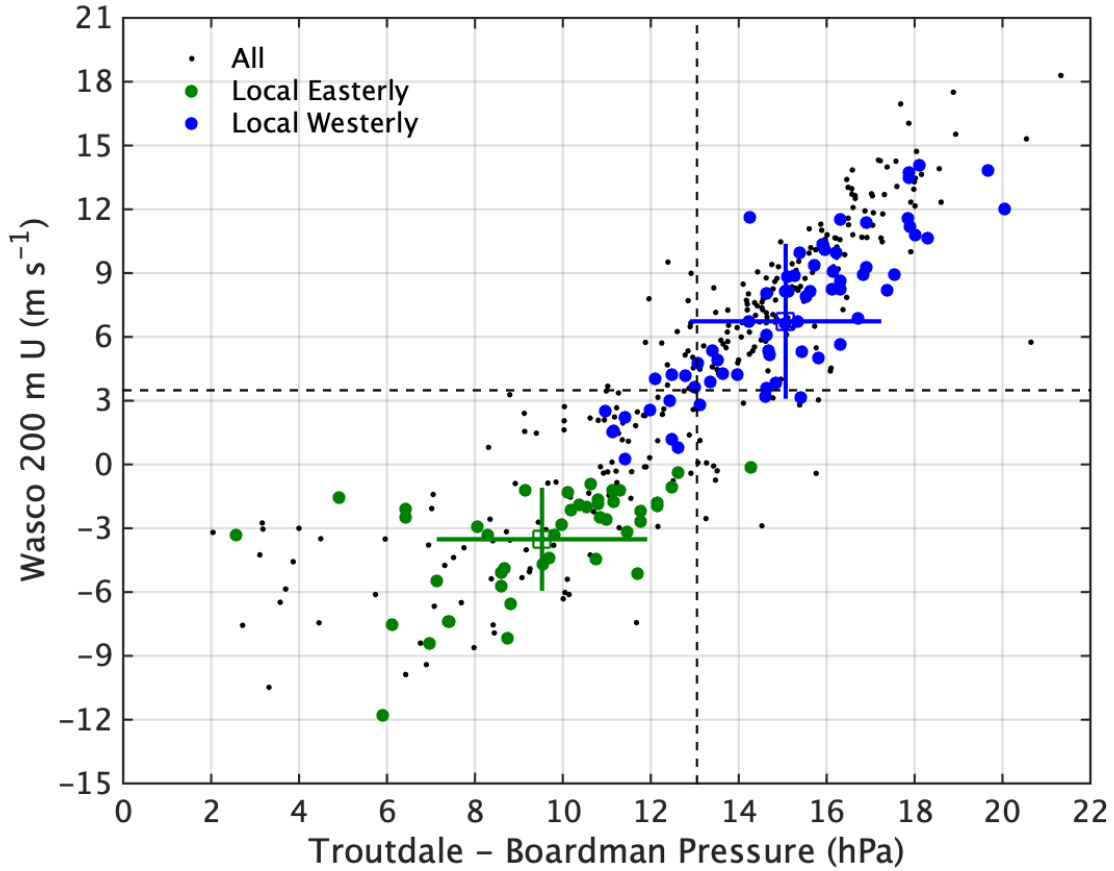


**FIGURE 5** Scatter plot of observed pressure differences at the surface between the Troutdale and Boardman sites and 200 m zonal wind speed (U) at Wasco. The values are daily averages for all days (*black dots*), local easterly days (*green circles*), and local westerly days (*blue circles*). The vertical and horizontal black dashed lines indicate mean values of the pressure difference and zonal wind speed, respectively. The average and one standard deviation values for easterly and westerly days are shown in squares and bars, respectively.

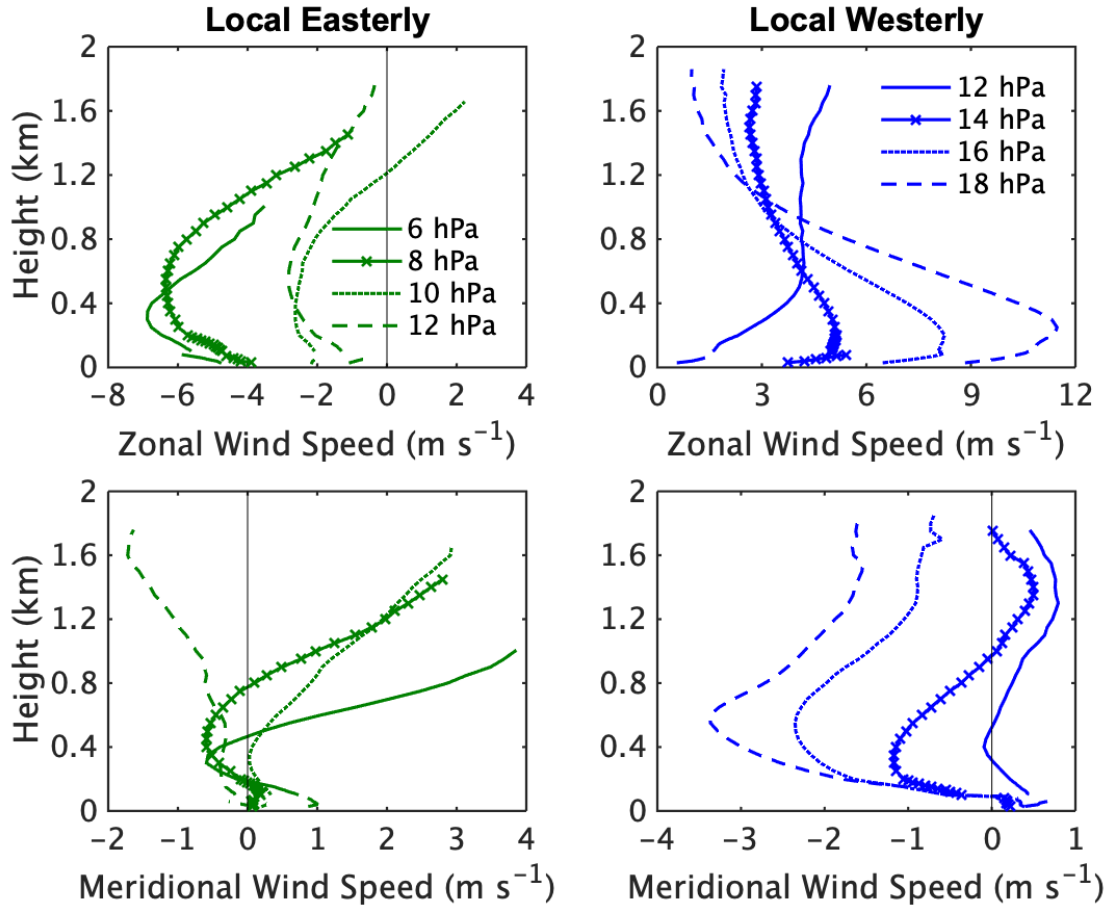


**FIGURE 6** Averaged observed vertical profiles of zonal (*top*) and meridional (*bottom*) wind speeds for easterly local days (*left*) and westerly local days (*right*) at Wasco for different surface pressure differences between Troutdale and Boardman. The mean pressure difference between Troutdale and Boardman was 13.05 hPa. The standard deviation bars are not shown for clarity.

#### 4.1.2 Troutdale

A scatter plot of observed pressure differences between Troutdale and Boardman and 200 m zonal wind speed at Troutdale at daily timescales is shown in Figure 7. The pressure differences were calculated from the microbarographs data, and the wind speed from the RWP data. The days were classified as local easterly (83 days) and local westerly (51 days) based on those determined from the wind data at Troutdale. The average ( $\pm$ standard deviation) pressure difference between Troutdale and Boardman was  $13.05 \pm 3.56$  hPa during the study period, and  $15.05 \pm 1.48$  hPa and  $10.02 \pm 2.76$  hPa, respectively, during locally forced westerly and easterly days. The average 200 m zonal wind speed at Troutdale was  $-2.40 \pm 5.80$  m s<sup>-1</sup>, while during locally forced westerly and easterly flow days it was  $1.45 \pm 0.66$  m s<sup>-1</sup> and  $-6.99 \pm 5.57$  m s<sup>-1</sup>, respectively. The zonal wind speed at 200 m showed a remarkably good correlation with the pressure difference during local easterly days, for a pressure difference lower than  $\sim 12$  hPa. For a pressure difference of between 12 and 15 hPa, both easterly and westerly winds of weaker magnitude were observed.

The 200 m zonal wind speed during local westerly days did not exhibit a relationship to the zonal pressure gradient. This suggests the controls of the mountain gap (and topography) affected the easterly winds through the pressure gradient at Troutdale. Scatter plots between 200 m zonal wind speed at Troutdale showed no relationship to the pressure difference between Hood River and Wasco.

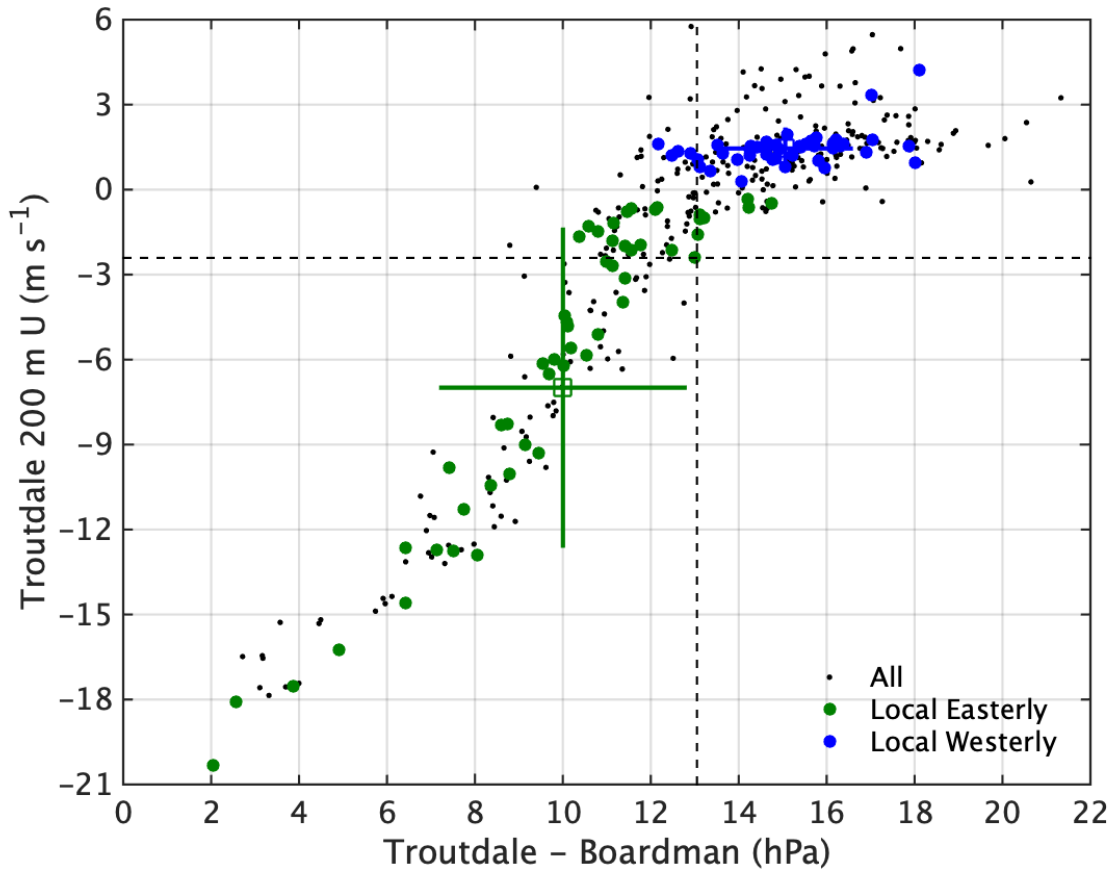


**FIGURE 7** Scatter plot of observed pressure differences at the surface between Troutdale and Boardman sites and 200 m zonal wind speed ( $U$ ) at Troutdale. The values are daily averages for all days (*black dots*), local easterly days (*green circles*), and local westerly days (*blue circles*) at Troutdale. The vertical and horizontal black dashed lines indicate mean values of the pressure difference and zonal wind speed, respectively. The averages and one standard deviation values for easterly and westerly days are shown in the square and bars, respectively.

The locally forced easterly and westerly days at Troutdale were further classified based on the pressure differences between Troutdale and Boardman in bins from 0 to 22 hPa every 2 hPa with a width of 2 hPa. The average profiles of zonal and meridional components of winds at Troutdale for different pressure differences between Troutdale and Boardman are shown in Figure 8. The numbers of samples for locally forced easterly days were 9, 16, 13, and 8 for pressure differences of 8, 10, 12, and 14 hPa, respectively. The numbers of samples for locally forced westerly days were 4, 17, 15, and 5 for pressure differences of 12, 14, 16, and 18 hPa, respectively.

Both easterly and westerly winds occurred for pressure differences of 12 and 14 hPa. During both local easterly and westerly days, the winds in the boundary layer were from the north. The zonal wind speed at Troutdale on average did not exhibit a diurnal cycle for the local days, local easterly days, or local westerly days. This was not surprising given the marine forced climate observed at Troutdale.

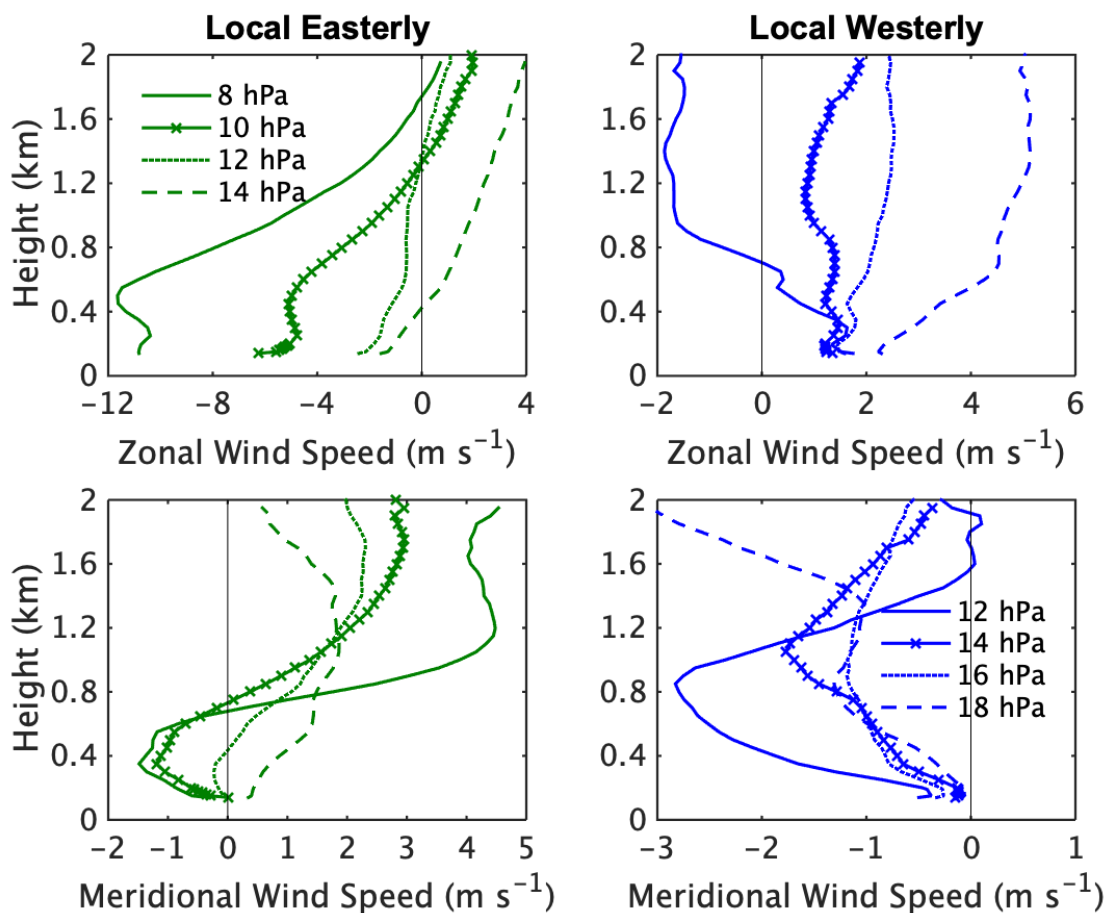


**FIGURE 8** Averaged observed vertical profiles of zonal (*top*) and meridional (*bottom*) wind speeds for easterly local days (*left*) and westerly local days (*right*) at Troutdale for different surface pressure differences between Troutdale and Boardman. The mean pressure difference between Troutdale and Boardman was 13.05 hPa. The standard deviation bars are not shown for clarity.

### 4.1.3 Boardman

The scatter plot of daily average zonal wind speed at 200 m at Boardman and the pressure differences between Troutdale and Umatilla is shown in Figure 9. The average ( $\pm$ standard deviation) pressure difference between Troutdale and Umatilla was  $17.79 \pm 3.43$  hPa during the study period, and  $20.05 \pm 2.25$  hPa and  $15.82 \pm 1.71$  hPa, respectively, during locally forced westerly and easterly days. The average 200 m zonal wind speed at Boardman was  $3.27 \pm 4.39$  m s<sup>-1</sup>, while during locally forced westerly and easterly flow days it was  $4.19 \pm 2.72$  m s<sup>-1</sup> and  $-1.41 \pm 0.68$  m s<sup>-1</sup>,

respectively. On average, the locally forced easterly days had much weaker winds than the locally forced westerly days.

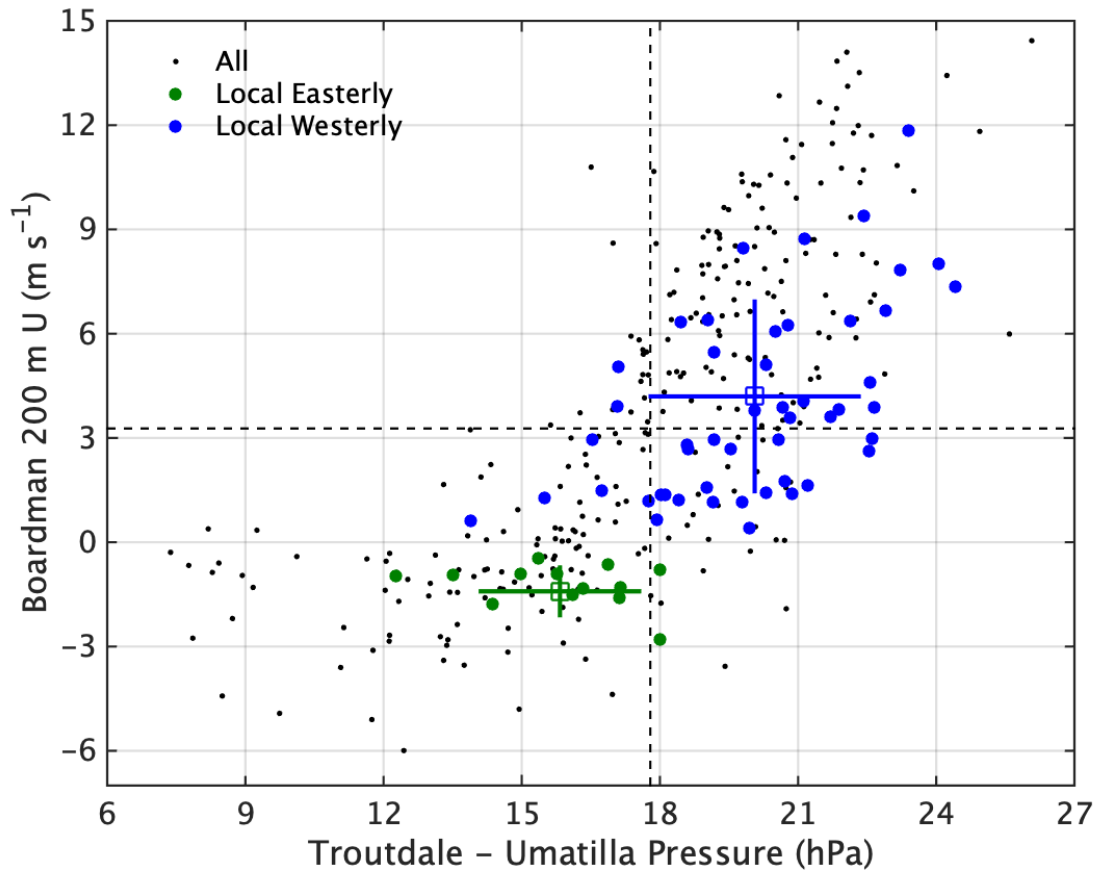


**FIGURE 9** Scatter plot of pressure difference at the surface between Troutdale and Umatilla sites and 200 m zonal wind speed (U) at Boardman. The values are daily averages for all days (*black dots*), local easterly flow days (*green circles*), and local westerly flow days (*blue circles*). The vertical and horizontal black dashed lines indicate mean values of the pressure difference and wind speed, respectively. The average and one standard deviation values for easterly and westerly days are shown in squares and bars, respectively.

Although having much scatter (variability), the zonal winds increased in magnitude with an increase in the pressure difference for the local westerly days. The local easterly days occurred when the pressure difference was less than ~18 hPa; however, these cases showed no relationship between the zonal wind speed and zonal pressure difference. The 200 m zonal wind speed at Boardman exhibited a similar relationship for the pressure difference between Hood River and Umatilla but exhibited no systematic (linear or otherwise) relationship with the pressure difference between Wasco and Umatilla.

The average profiles of zonal and meridional components of winds at Boardman for different pressure differences between Troutdale and Umatilla are shown in Figure 10. The number of samples for locally forced easterly days was 5 and 4 for 16 hPa and 18 hPa pressure differences, respectively. The number of samples for locally forced westerly flow days was 10, 19, 12, and 4 for 18 hPa, 20 hPa, 22 hPa, and 24 hPa pressure differences, respectively. For a pressure difference of 18 hPa, both local easterly and westerly flows were observed. Similar to Wasco, wind shear and veer was present in both zonal and meridional wind for all the pressure difference values. Winds at Boardman were on average weaker than those at Wasco for both easterly and westerly locally forced days. One notable difference at Boardman was that the winds below 2 km were from the north-northeast during the locally forced easterly days, and were from the southwest during locally forced westerly days. Hence the flow was from the mountains to the northeast during local easterly days and was from the channel during the westerly days. In addition, the magnitudes of the meridional components of the winds were comparable to the zonal components at all levels, suggesting the importance of north-south gradients in the pressure fields and north-south orientation of topography in determining the winds. A wind jet was also present in all of the profiles; however, the location of the nose was much higher than in Wasco.

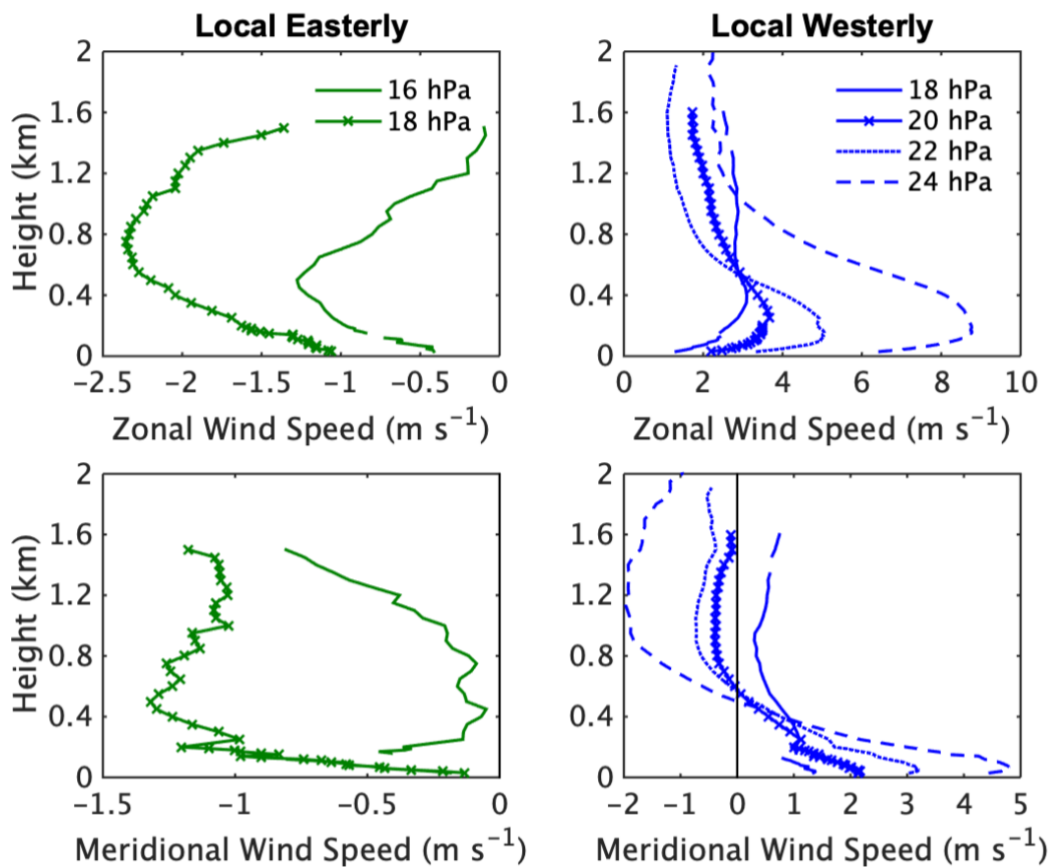


**FIGURE 10** Averaged vertical profiles of zonal (*top*) and meridional (*bottom*) RWP wind speeds for easterly local days (*left*) and westerly local days (*right*) at Boardman for different pressure differences between Troutdale and Umatilla. The standard deviation bars are not shown for clarity.

## 4.2 DIURNAL TIMESCALES

This section examines the diurnal cycle of the relationship between zonal wind speed and the zonal pressure gradient at Wasco and Boardman. Troutdale is not examined because the variables were not related at daily timescales.

### 4.2.1 Wasco

The average diurnal cycle of zonal wind speed during all local days (Figure 11a) showcased weak winds with little diurnal variability due to averaging easterly and westerly days. On average, strong zonal winds ( $>3 \text{ m s}^{-1}$ ) were observed from midnight to 4 a.m. below 500 m. The average diurnal cycle of zonal wind speed during local easterly days exhibited weak winds during the entire day except from 4 p.m. to midnight below 1 km. The average diurnal cycle of zonal wind speed during local westerly days exhibited a strong diurnal cycle with high winds below 1 km from 6 p.m. to 7 a.m., and weak winds during the daytime due to mixing. To probe whether the changes in the daily average zonal wind speeds exhibit any systematic diurnal variations, the difference between the average diurnal cycle during local easterly (and westerly) days and the average diurnal cycle from all the local days was examined (Figure 11d). For both local easterly and westerly days, the change in zonal wind speed from the average was highest between 4 p.m. and midnight, with an accompanied weak increase from midnight to 8 a.m. Collectively, this figure shows a diurnal variation in zonal wind to be present at the site during both local easterly and local westerly days, with strengthening of the winds more during the nighttime than during the daytime due to changes in pressure gradients.

The diurnal cycle of the zonal pressure gradient and the 200m zonal wind speed at Wasco were examined next (Figure 12). The zonal pressure gradient was almost constant from 4 p.m. to midnight, with a minimum at 7 a.m. The minimum of zonal wind speed was at 1 p.m. with an almost constant value from 8 p.m. to midnight. This suggests the diurnal cycle of the zonal pressure gradient leads the diurnal cycle of the zonal wind speed by six hours. The phase diagram between the zonal pressure gradient and the 200 m zonal wind speed demonstrates a decrease in both quantities from midnight to 7 a.m., an increase in the pressure gradient and decrease in the winds from 7 a.m. to 1 p.m., and an increase in the wind speed with no changes in the pressure gradient from 2 p.m. to midnight.

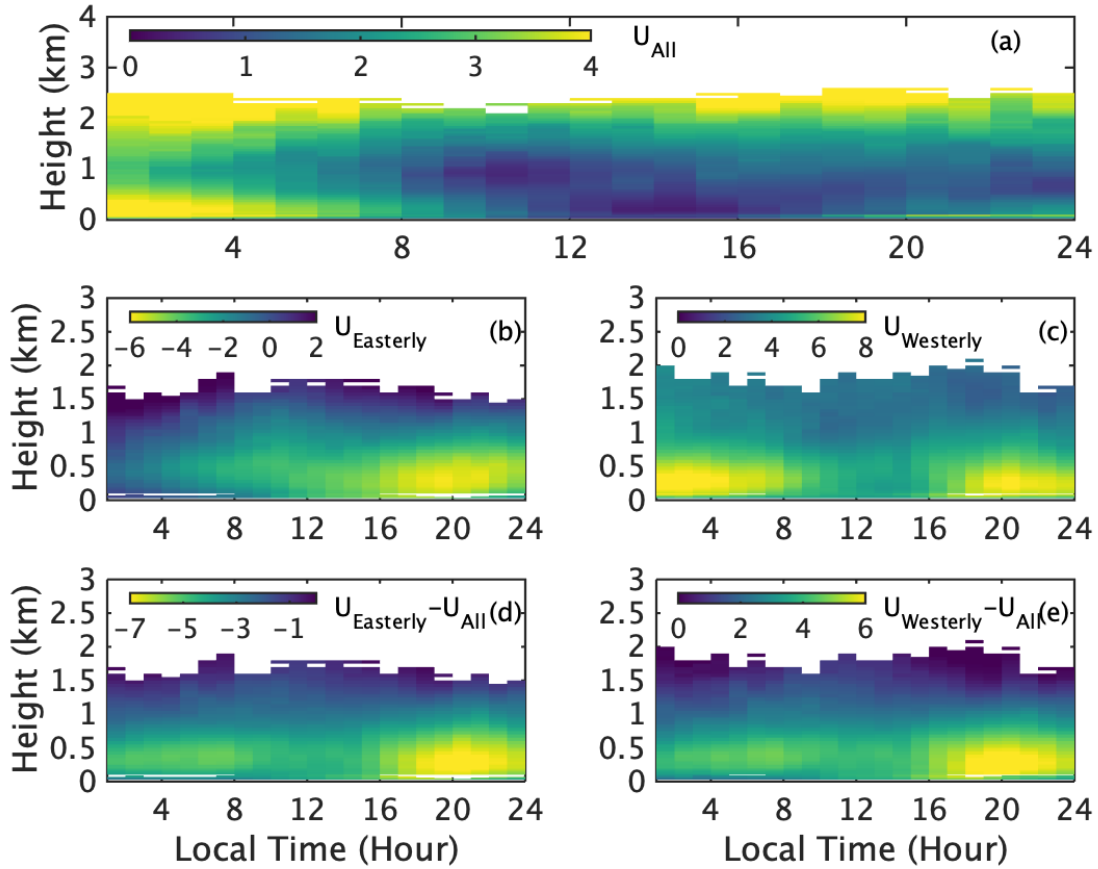


**FIGURE 11** (a) Average diurnal cycle of zonal wind speed during all locally forced days at Wasco; (b) average diurnal cycle of zonal wind speed during local easterly days at Wasco; (c) average diurnal cycle of zonal wind speed during local westerly days at Wasco; (d) average diurnal cycle of zonal wind speed during local easterly days at Wasco with averages shown in (a) removed, and (e) average diurnal cycle of zonal wind speed during local westerly days at Wasco with averages shown in (a) removed.

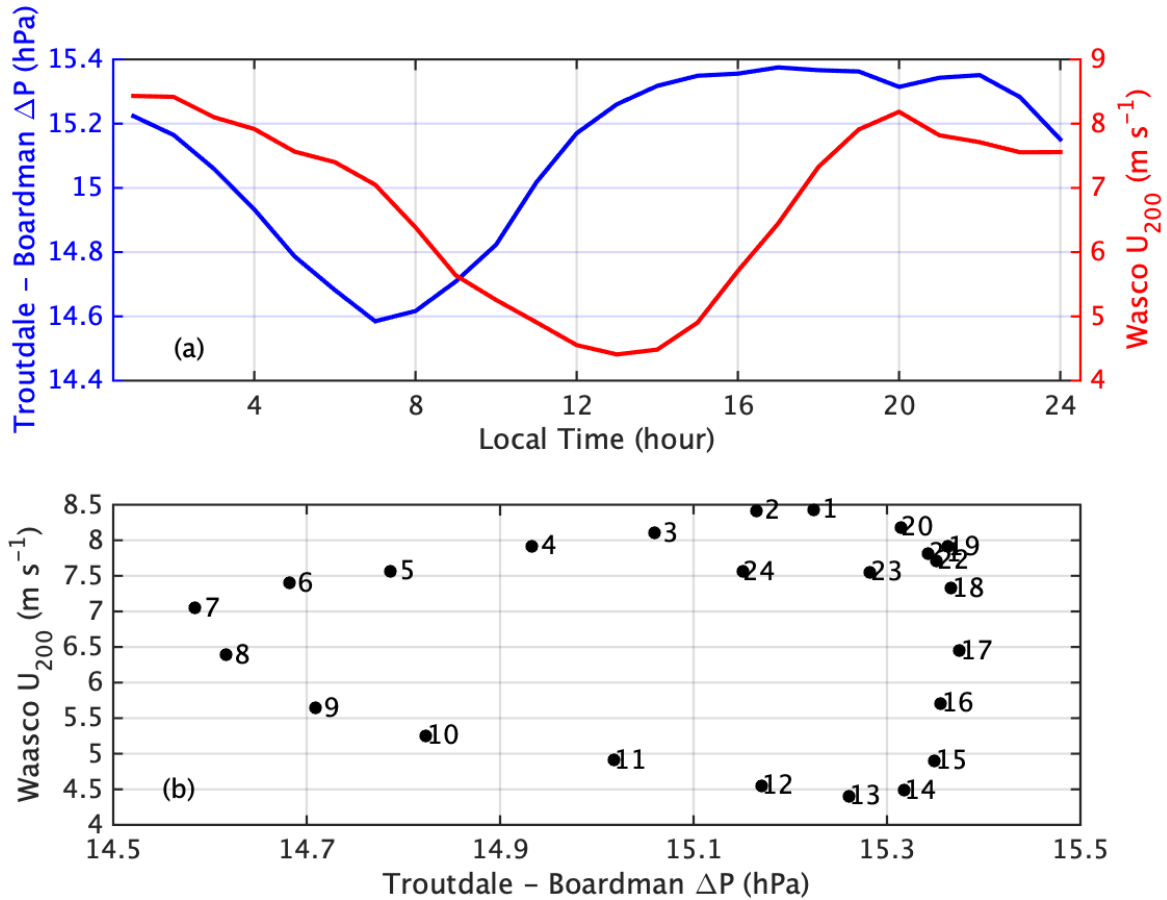


**FIGURE 12** (a) Average diurnal cycle of 200 m zonal wind speed ( $U_{200}$ ) at Wasco and difference between the surface air pressure at Troutdale and Boardman the during westerly days; (b) scatter plot between the average 200 m zonal wind speed and local zonal pressure gradient at Wasco during westerly gap flow days. The numbers indicate local time.

#### 4.2.2 Boardman

The average diurnal cycle of zonal wind speed during all local days at Boardman showed stronger winds during the nighttime hours and weaker winds during the daytime hours, consistent with diurnal heating (Figure 13). The increase in the wind speed during the nighttime was confined to below 500 m. Similar to Wasco, the average diurnal cycle of zonal wind speed during local easterly days showed stronger winds between 4 p.m. and midnight, and the diurnal cycle during local westerly days exhibited stronger winds during the entire nighttime. The difference between the average diurnal cycle of zonal wind speed during local easterly (and westerly) days and that from all the local days showed stronger winds during the nighttime than during the daytime, suggesting the increase in pressure gradient affected nighttime winds more severely than the daytime winds. The magnitude of differences in Figure 11d and 11e suggest a greater impact of the diurnal cycle during the local easterly days compared with the mean than during local westerly days at Boardman.

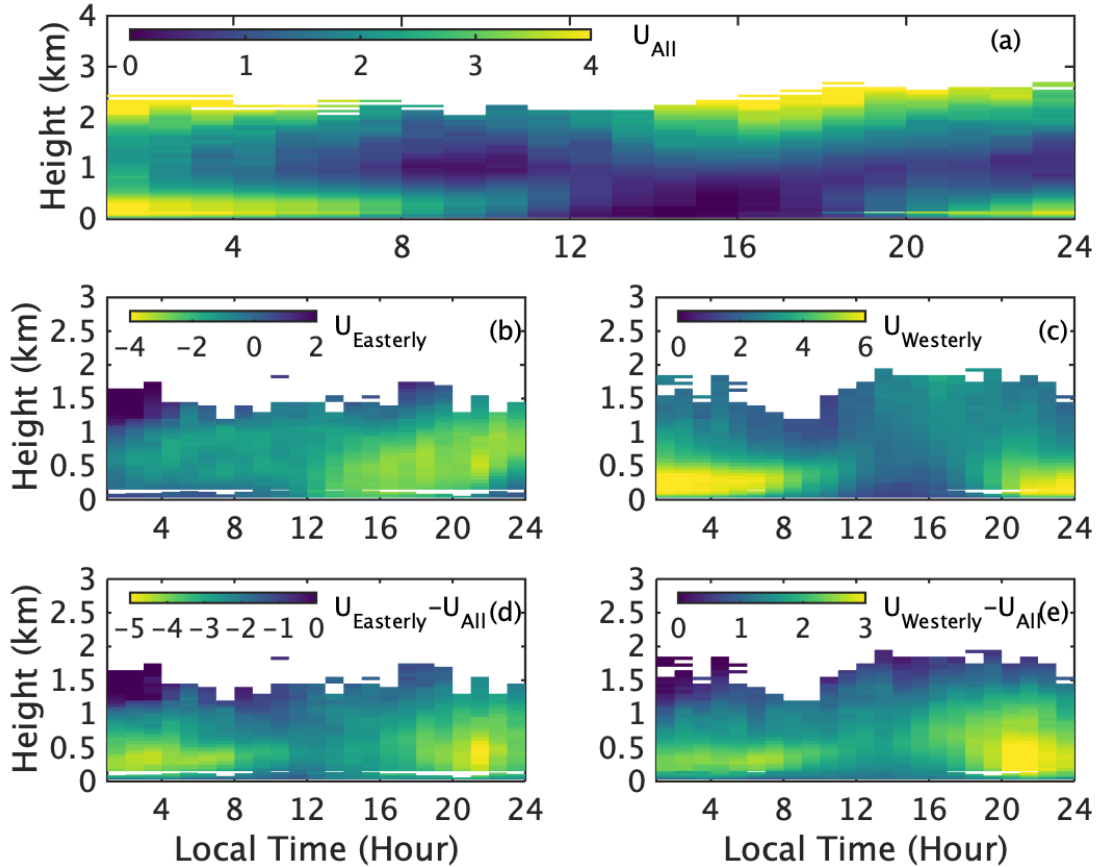


**FIGURE 13** (a) Average diurnal cycle of zonal wind speed ( $U$ ) during locally forced days at Boardman; (b) average diurnal cycle of zonal wind speed during local easterly days at Boardman; (c) average diurnal cycle of zonal wind speed during local westerly days at Boardman; (d) difference between  $b$  and  $a$ ; (e) difference between  $c$  and  $a$ .

The diurnal cycle of the 200 m zonal wind speed and the zonal pressure gradient at Boardman were examined next (Figure 14). The zonal pressure gradient exhibited a minimum at 7 a.m. and a maximum at 9 p.m., while the 200 m zonal wind speed exhibited a minimum at 2 p.m. and maximum at 1 a.m. These diurnal cycles were vastly different than those at observed at Wasco (Figure 12). The phase diagram between the zonal pressure gradient and the 200 m zonal wind speed shows a much different structure at Boardman than at Wasco, as well. The pressure decreased from 9 p.m. to 6 a.m., with little change in the wind speeds, followed by an increase in the pressure and decrease in winds from 7 a.m. to 2 p.m., and an increase in pressure gradient and increase in winds from 2 p.m. to 8 p.m.

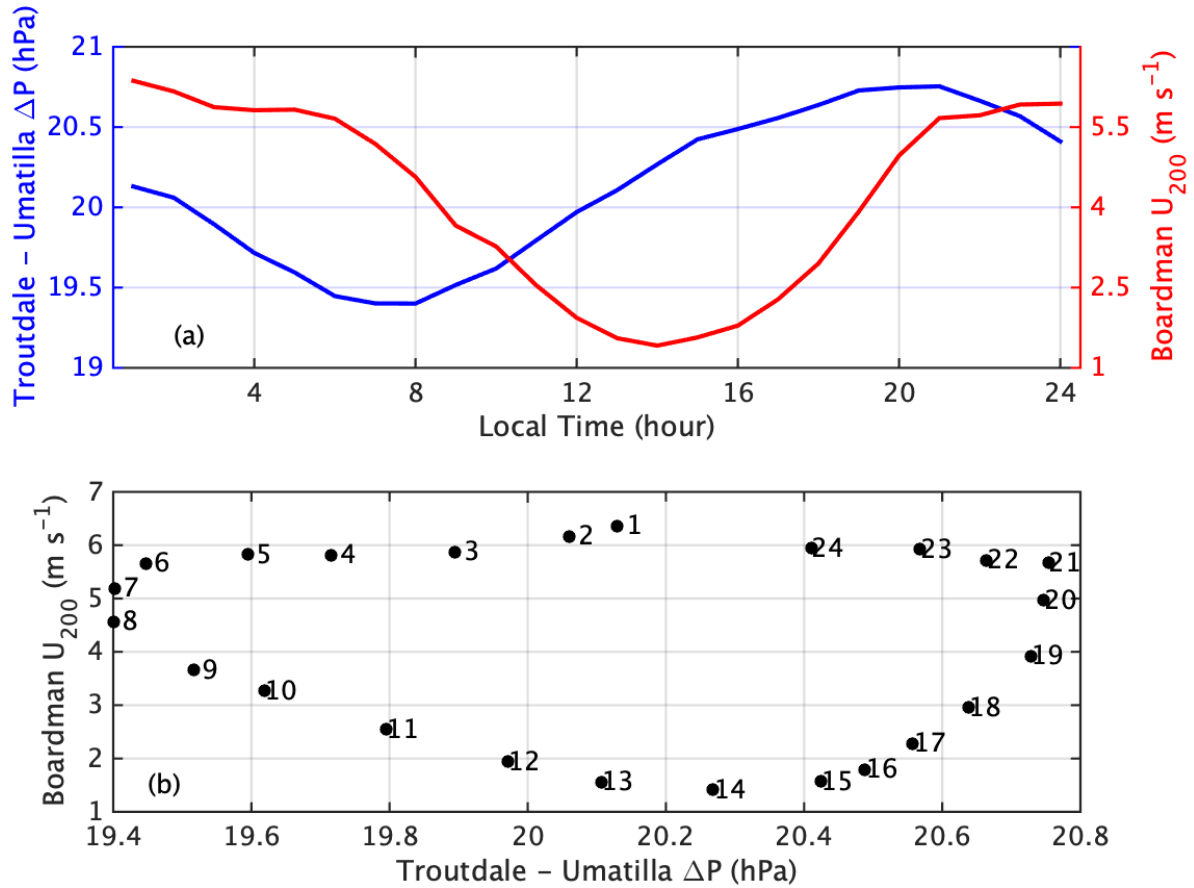


**FIGURE 14** *Top:* Average diurnal cycle of the 200 m zonal wind speed ( $U_{200}$ ) and difference between surface air pressure at Troutdale and Umatilla during westerly gap flow days. *Bottom:* Scatter plot between the 200 m zonal wind speed at Boardman, and pressure differences between Troutdale and Umatilla. The numbers indicate local time in hours.

## 5 PERFORMANCE OF THE HRRR MODEL

Due to the higher number of samples and the linear relationship between the zonal wind speed and the pressure difference, we assessed the accuracy of the HRRR model at forecasting them. Of a total of 153 local easterly and westerly days at Wasco, the reforecast HRRR model data was available on 64 days, 40 of which were westerly and 24 easterly. Although model simulations were made in the control and experimental setups at two horizontal resolutions, the differences between the forecasted winds in the control vs. experimental setups were small for these types of events. A scatter plot showcasing this is included in the supplemental material; hence, below, we only focus on the output from the control runs for two model resolutions.

A scatter plot between the 200 m zonal wind speed at Wasco and the pressure differences between Troutdale and Boardman from observations and as simulated by HRRR is shown in Figure 15. For the 3 km horizontal resolution simulation, the model overestimated the zonal wind speed for the same horizontal pressure difference, while simulating closer to the observed wind speeds for the higher resolution (750 m) simulation. The HRRR-3km mode simulation did not

simulate zonal pressure differences greater than 16 hPa that were observed on 16 days, and the HRRR-750m model simulation did not simulate zonal pressure differences greater than 19 hPa that were observed on 2 days. Zonal pressure differences smaller than 8 hPa were observed only on 5 days, while they were simulated on 17 days by the HRRR-3km simulations. For the same zonal pressure difference, the HRRR model in 3 km setup overpredicted the zonal wind speed at 200 m during local westerly days and underpredicted the 200 m zonal wind speed during local easterly days. However, the HRRR model in 750 m setup accurately captured the magnitude of zonal wind speed for same zonal pressure difference for both easterly and westerly local days. The plot highlights the improvement in the HRRR model-predicted zonal wind speed due to the increase in horizontal resolution.

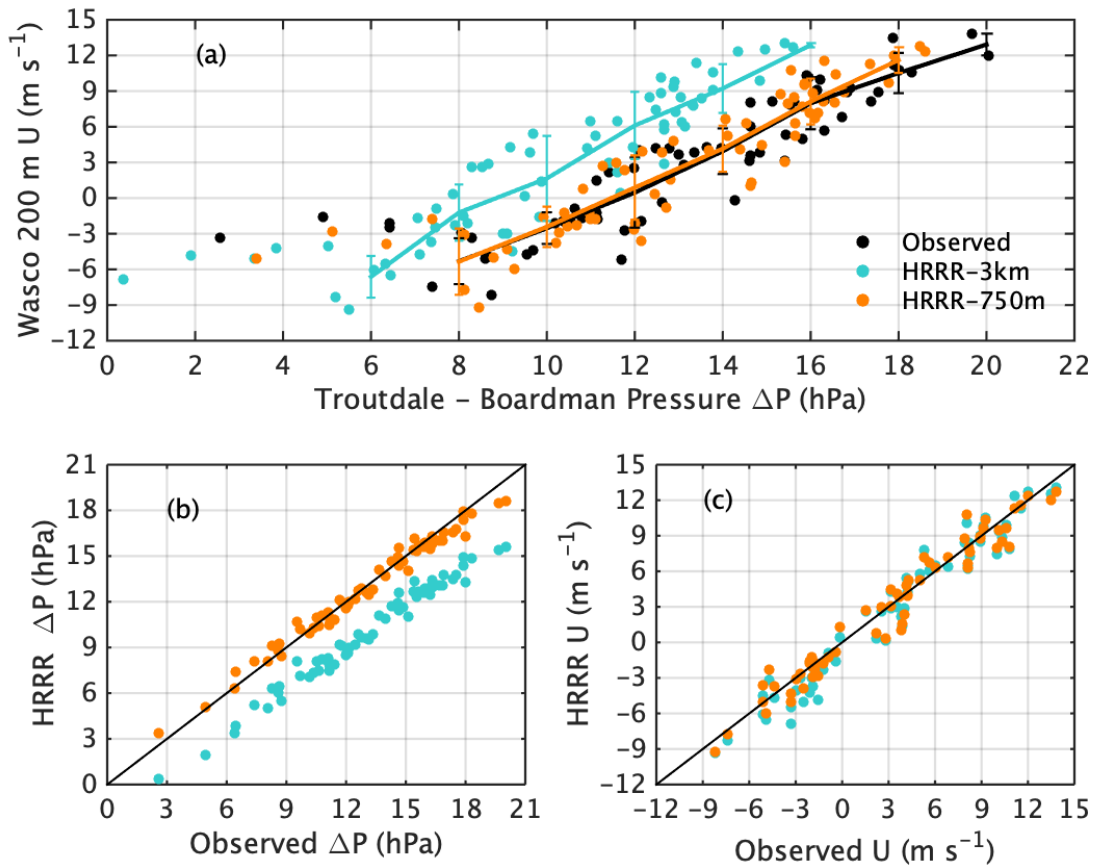
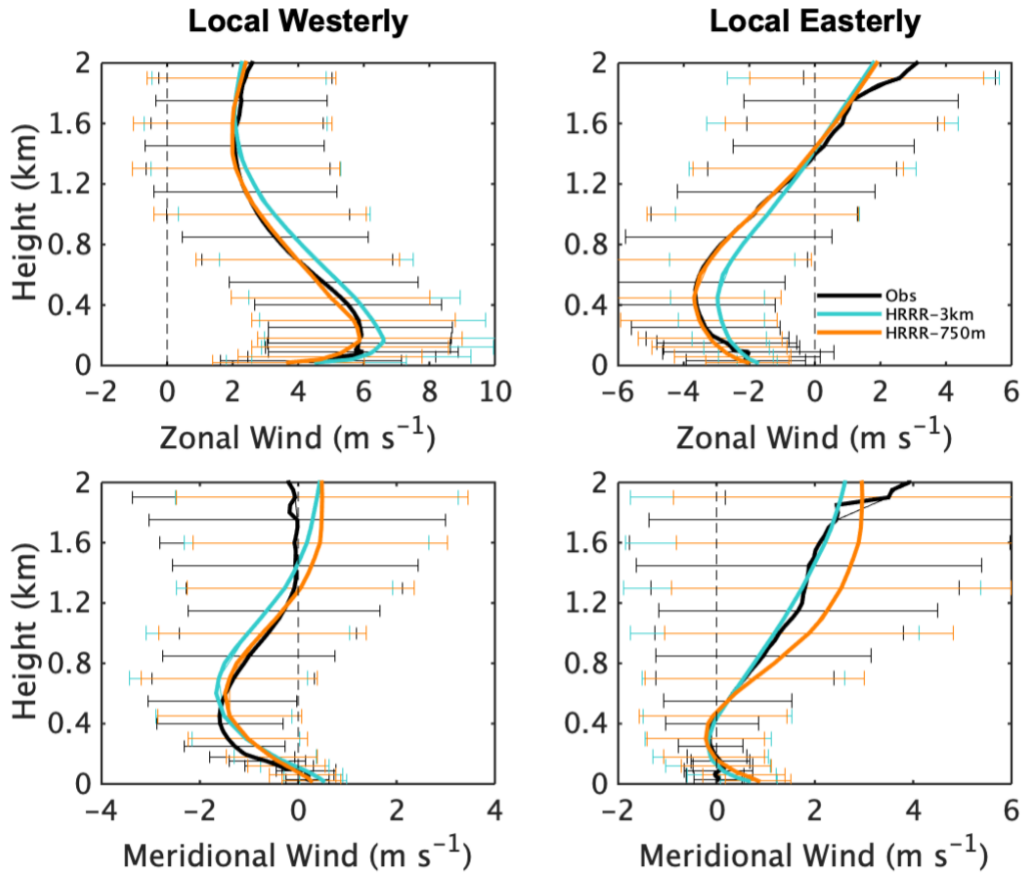


**FIGURE 15** (a) Scatter plot of daily averaged pressure differences between Troutdale and Boardman and 200 m zonal wind speed ( $U$ ) during local days at Wasco from observations, simulated by HRRR-3km and by HRRR-750m. (b) Scatter plot between observed and HRRR model-simulated pressure differences between Troutdale and Boardman during local days. (c) Scatter plot between observed and HRRR-simulated 200 m zonal wind speed at Wasco during local days.

The scatter plot between the observed and model-simulated zonal pressure difference (Figure 15b) and observed and modeled zonal wind speed at 200 m at Wasco (Figure 15c) demonstrates that although the model underestimated the zonal pressure difference in the 3 km setup, it nevertheless simulated the zonal wind speed with reasonable accuracy in both setups. The RMSDs between the observed and model-simulated zonal pressure difference were 3.14 hPa for HRRR-3km and 0.57 hPa for the HRRR-750m, while the RMSDs between the observed and model-simulated zonal wind speed at 200 m were 1.40 m s<sup>-1</sup> for HRRR-3km and 1.20 m s<sup>-1</sup> for HRRR-750m. The RMSDs between the observed and model simulated zonal wind speed (and zonal pressure gradient) were similar for both easterly and westerly gap flow days for both model simulations, suggesting the differences were independent of the meteorological conditions. Hence, the HRRR model's ability to simulate zonal pressure gradient improved due to increase in the horizontal resolution from 3 km to 750m, but did not result in substantial improvement in the daily averaged zonal wind speeds. With an improvement in simulating the zonal pressure gradient and negligible changes in simulating zonal wind speed with the high-resolution simulation, our analysis points to a complex interplay between different components of the model physics in simulating the meteorology.

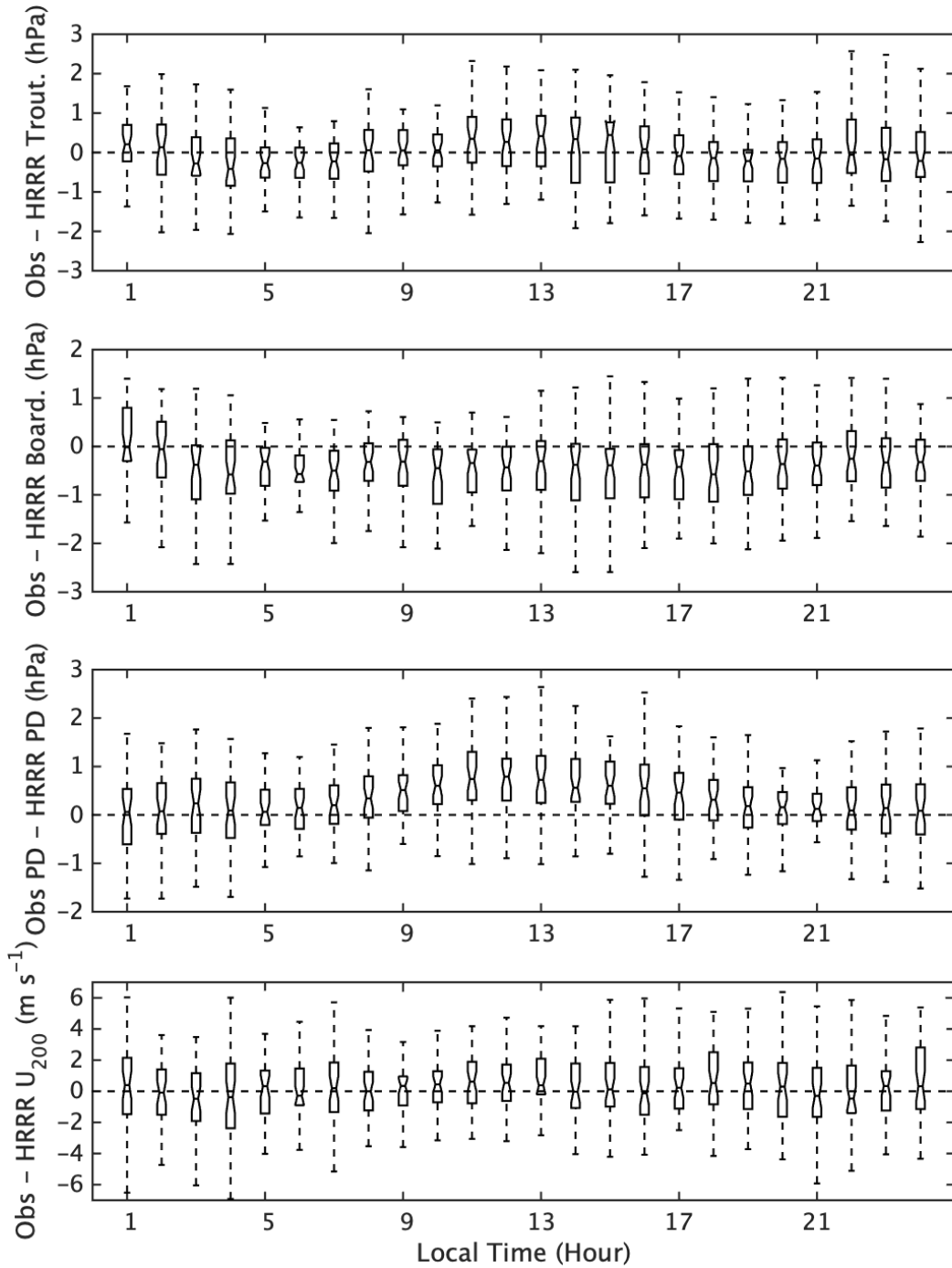
Values of zonal pressure differences of 7–17 hPa were both observed and simulated by the HRRR model in both setups. For a zonal pressure difference of 7–17 hPa, 20 (32), 13 (41), and 20 (36) samples were available from the observations, HRRR-3km, and HRRR-750m for local easterly (westerly) days, respectively. The observed pressure difference between Troutdale and Boardman for this subset during easterly (westerly) days was  $10.31 \pm 1.72$  hPa ( $14.65 \pm 1.68$ ), and the modeled pressure differences for the HRRR-3km and HRRR-750 m were  $8.14 \pm 0.88$  hPa ( $10.15 \pm 1.49$ ) and  $12.06 \pm 1.98$  hPa ( $14.62 \pm 1.70$ ), respectively.

Figure 16 shows the average wind profiles from the observations and the HRRR-3km and HRRR-750m models during local easterly and westerly days for zonal pressure differences of 7–17 hPa. On average, an improvement in the HRRR model's ability to simulate zonal wind speed due to increased horizontal resolution can be seen for both easterly and westerly days. The averaged profiles of zonal wind speed indicate a reduction in magnitude during local westerly days and an increase in magnitude during local easterly days due to an increase in resolution, which resulted in better agreement with the observed profiles. The increase in the HRRR model's horizontal resolution had minimal impact on the simulated meridional wind speeds. The figure suggests the model's representation of the zonal pressure gradient, which was largely determined by the representation of the terrain in the model, was responsible for the inaccuracies in forecasted winds.



**FIGURE 16** Zonal (*top*) and meridional (*bottom*) wind speeds as observed and simulated with the HRRR-3km and HRRR-750m models for local westerly (*left*) and local easterly (*right*) days with pressure differences between Troutdale and Boardman of 7–17 hPa. The horizontal bars denote one standard deviation from the mean.

We analyzed the performance of the HRRR model simulating the diurnal zonal pressure gradient and 200 m zonal wind speed during locally forced westerly gap flow days at Wasco. The difference between HRRR-740m-simulated and observed surface air pressure at Troutdale and Boardman, along with the model-simulated and observed zonal pressure difference and 200m zonal wind speed, are shown in Figure 17. The HRRR-750m model does reasonably well simulating the surface air pressure at Troutdale, with small variations ( $< 1$  hPa) in median values throughout the day. Apart from 1 a.m. values, the model overestimates the surface air pressure at Boardman at all times. Due to the overestimation of the surface air pressure at Boardman, the model underestimates the zonal pressure difference, with the underestimation the greatest between 9 a.m. and 5 p.m. Despite this underestimation in the zonal pressure difference, the model does reasonably well simulating the 200 m zonal wind speeds, with the median values of the model error being very close to zero for the entire range of the diurnal cycle. Locally forced westerly gap flow days at Wasco were observed for a zonal pressure difference of 12 to 20 hPa. Because Figure 17 depicts all of these days, the range whiskers and the 25th to 75th percentile box lengths denote the ranges of the weather conditions rather than the model errors during those times.



**FIGURE 17** For the locally forced westerly days, box plots showing the diurnal cycle of surface air pressure at Troutdale, surface air pressure at Boardman, the difference between surface air pressure at Troutdale and Boardman, and the 200 m zonal wind speed ( $U_{200}$ ). Values are as observed (*black*) and as simulated by the HRRR model in 750 m spatial resolution (*blue*). For clarity, just the values for every other hour are shown.

The HRRR-750m model's efficacy at simulating the covariability of the zonal pressure difference and the 200 m zonal pressure gradient is depicted in Figure 18. The model does reasonably well at simulating the diurnal cycle of the covariability of the zonal pressure difference and the zonal wind speed from midnight to 7 a.m.; however, it fails to capture the decrease in the 200 m zonal wind speed with an increase in the zonal pressure difference from 7 a.m. to 2 p.m. Hence, rather than simulating a triangular shape of the phase diagram, the model simulates an elliptical shape of the phase diagram. This points to the HRRR model's inability to simulate some of the boundary layer mixing processes during the daytime.

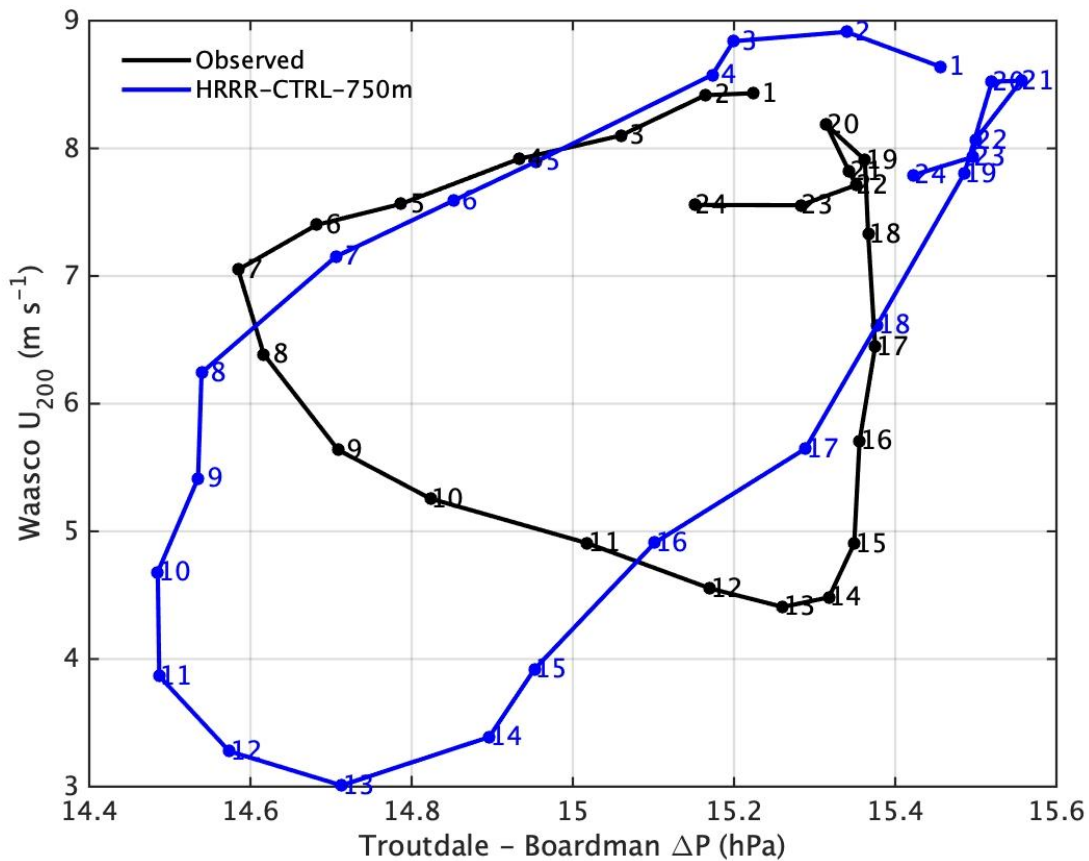


**FIGURE 18** Phase diagram between the zonal pressure gradient and the 200 m zonal wind speeds ( $U_{200}$ ) at Wasco during locally forced westerly gap flow days as observed (*black*) and as simulated by the HRRR model at 750 m spatial resolution.

## 6 SUMMARY AND DISCUSSION

Observations collected at five locations along the Columbia River during the Second Wind Forecasting Improvement Project (WFIP2) were analyzed to understand the relationship between zonal pressure gradient and zonal winds during locally forced gap flow events at daily and hourly

timescales. Locally forced and synoptically forced events were identified using an objective criterion based on the wind speed at 1.5 km. The primary findings of the analysis were:

1. The 200 m zonal wind speed at Wasco exhibited a linear relationship with the pressure gradient between Troutdale and Boardman (202.16 km apart) on daily timescales, with the zonal winds getting stronger with the pressure gradient for both easterly and westerly local days. The changes in the zonal wind speed due to changes in the pressure gradient were mostly from 4 p.m. to midnight during easterly days and during the nighttime hours during westerly days.
2. The 200 m zonal wind speed at Troutdale exhibited a linear relationship with the pressure gradient between Troutdale and Boardman during local easterly days on daily timescales, but did not exhibit any such relation during local westerly days. The zonal winds at Troutdale also did not exhibit any distinct diurnal cycle.
3. The zonal wind speed at Boardman exhibited a weak linear relationship with the pressure difference between Troutdale and Umatilla during both local easterly and westerly days on daily timescales. The zonal wind speed at Boardman exhibited a distinct diurnal cycle during both easterly and westerly days, with changes in the zonal wind speed due to the changes in pressure gradient mostly occurring during nighttime hours.
4. Increase in the horizontal resolution from 3 km to 750 m led to significant improvement in model representation of pressure differences between Troutdale and Boardman; however, that led to a minimal improvement in simulating 200 m zonal wind speed.
5. The HRRR model failed to capture the co-variability (phase diagram) between the zonal pressure difference and 200 m zonal wind speed by simulating an elliptical shaped phase rather than the observed triangular shape. The model errors during the daytime (7 a.m.–2 p.m.) point toward its inability to simulate boundary layer mixing processes.

During local easterly days, the 200 m zonal wind at Boardman exhibited little variability with no clear dependence on the zonal pressure gradient. A clearer dependence was found at Wasco and at Troutdale, where the zonal wind speed exhibited a linear relationship with the zonal pressure gradient. This was consistent with the blocking of the easterly flow by the Cascade Mountains and a Venturi-type effect at Troutdale. The 200 m zonal wind speed during westerly gap flow days showed no relation with the zonal pressure gradient at Troutdale, exhibited a strong linear relationship with the zonal pressure gradient at Wasco, and had a weaker relationship with the zonal pressure gradient at Boardman. This suggests the Venturi-type effect east of the Cascade mountains during local westerly gap flow days is less pronounced and affected by the terrain as it progresses eastward.

The range of daily averaged 200 m zonal wind speed simulated by the HRRR model in both setups was similar to the range observed, but the daily averaged zonal pressure difference was underestimated by the model in the 3 km setup. The agreement of the model-forecasted winds with the observed, even with the forecasted lower than observed zonal pressure difference, suggests some compensation of model errors. The HRRR reforecast simulations used in this work did not utilize additional data assimilation, but some portion of the errors may be inherited from the 13 km Rapid Refresh, which was used to initialize the HRRR. That said, some portion of the errors were likely due to inaccurate representation of terrain in the model or model physics/numerics.

## REFERENCES

- Adler, B., J. M. Wilczak, L. Bianco, et al., 2021: Observational Case Study of a Persistent Cold Pool and Gap Flow in the Columbia River Basin, *J. Appl. Meteor. Climatol.*, 60(8), 1071–1090.
- Arthur, R.S., K.A. Lundquist, Olson, J.B. 2021: Improved Prediction of Cold-Air Pools in the Weather Research and Forecasting Model Using a Truly Horizontal Diffusion Scheme for Potential Temperature, *Mon. Wea. Rev.*, 149(1), 155–171.
- Banta, R.M., Y.L. Pichugina, W.A. Brewer, et al., 2020: Characterizing NWP Model Errors Using Doppler-Lidar Measurements of Recurrent Regional Diurnal Flows: Marine-Air Intrusions into the Columbia River Basin, *Mon. Wea. Rev.*, 148(3), 929–953.
- Banta, R.M., Y.L. Pichugina, L.S. Darby, et al., 2021: Doppler Lidar Evaluation of HRRR Model Skill at Simulating Summertime Wind Regimes in the Columbia River Basin during WFIP2, *Wea. Forecasting*, 36(6), 1961–1983.
- Benjamin, S.G., S.S. Weygandt, J.M. Brown, et al., 2016: A North American Hourly Assimilation and Model Forecast Cycle: The Rapid Refresh. *Mon. Wea. Rev.*, 144, 1669–1694, <https://doi.org/10.1175/MWR-D-15-0242.1>.
- Bianco, L., I.V. Djalalova, J.M. Wilczak, et al., 2019: Impact of Model Improvements on 80 m Wind Speeds During the Second Wind Forecast Improvement Project (WFIP2), *Geosci. Model Dev.*, 12, 4803–4821, <https://doi.org/10.5194/gmd-12-4803-2019>.
- Bianco, L., P. Muradyan, I. Djalalova, et al., 2021: Comparison of Observations and Predictions of Daytime Planetary-Boundary-Layer Heights and Surface Meteorological Variables in the Columbia River Gorge and Basin During the Second Wind Forecast Improvement Project, *Bound.-Layer Meteor.*, 1573–1472.
- Brewer, M.C., and C.F. Mass, 2014: Simulation of Summer Diurnal Circulations over the Northwest United States, *Wea. Forecasting*, 29, 1208–1228, <https://doi.org/10.1175/WAF-D-14-00018.1>

Colle, B.A., and C.F. Mass, 2000: High-Resolution Observations and Numerical Simulations of Easterly Gap Flow Through the Strait of Juan de Fuca on 9–10 December 1995, *Mon. Wea. Rev.*, 128, 2398–2422.

Draxl, C., R.P. Worsnop, G. Xia, et al., 2021: Mountain Waves Can Impact Wind Power Generation, *Wind Energy Sci.*, 6(1), 2366–7451.

Kalnay, E., M. Kanamitsu, R. Kistler, et al., 1996: The NCEP/NCAR 40-Year Reanalysis Project, *Bull. Amer. Meteor. Soc.*, 77, 437–472, [https://doi.org/10.1175/1520-0477\(1996\)077<0437:TNYRP>2.0.CO;2](https://doi.org/10.1175/1520-0477(1996)077<0437:TNYRP>2.0.CO;2).

Marquis, M., Wilczak, J., Ahlstrom, M., Sharp, J., Stern, A., Smith, J. C., & Calvert, S. 2011: Forecasting the Wind to Reach Significant Penetration Levels of Wind Energy, *Bulletin of the American Meteorological Society*, **92(9)**, 1159-1171

McCaffrey, K., J.M. Wilczak, L. Bianco, et al., 2019: Identification and Characterization of Persistent Cold Pool Events from Temperature and Wind Profilers in the Columbia River Basin, *J. Appl. Meteor. Climatol.*, <https://doi.org/10.1175/JAMC-D-19-0046.1>.

Neiman, P.J., D.J. Gottas, A.B. White, et al., 2018: A Real-Time Online Data Product that Automatically Detects Easterly Gap-Flow Events and Precipitation Type in the Columbia River Gorge, *J. Atmos. Oceanic Technol.*, 35, 2037–2052.

Nishiyama, R.T., and A.J. Bedard, Jr., 1991: A “Quad-Disc” Static Pressure Probe for Measurement in Adverse Atmospheres: With a Comparative Review of Static Pressure Probe Designs, *Rev. Sci. Instrum.*, 62, 2193–2204.

Olson, J. B., J.S. Kenyon, I. Djalalova, et al., 2019: Improving Wind Energy Forecasting Through Numerical Weather Prediction Model Development, *Bull. Amer. Meteor. Soc.*, 100, 11, 2201–2220, [10.1175/BAMS-D-18-0040.1](https://doi.org/10.1175/BAMS-D-18-0040.1).

Pichugina, Y.L., et al., 2019: Spatial Variability of Winds and HRRR–NCEP Model Error Statistics at Three Doppler-Lidar Sites in the Wind-Energy Generation Region of the Columbia River Basin. *J. Appl. Meteor. Climatol.*, 58, 1633–1656.

Pichugina, Y.L., R.M. Banta, W. Alan Brewer, et al., 2020: Evaluating the WFIP2 Updates to the HRRR Model Using Scanning Doppler Lidar Measurements in the Complex Terrain of the Columbia River Basin, *J. Renew. Sustain. Energy*, 12 (4), 1941–7012.

Reeves, H.D., and D.J. Stensrud, 2009: Synoptic-Scale Flow and Valley Cold Pool Evolution in the Western United States, *Wea. Forecasting*, 24, 1625–1643, <https://doi.org/10.1175/2009WAF2222234.1>.

Sharp, J.M., and C.F. Mass, 2002: Columbia Gorge Gap Flow: Insights from Observational Analysis and Ultra-High-Resolution Simulation, *Bull. Amer. Meteor. Soc.*, 83, 1757–1762, <https://doi.org/10.1175/BAMS-83-12-1757>.

Sharp, J., and C.F. Mass, 2004: Columbia Gorge Gap Winds: Their Climatological Influence and Synoptic Evolution, *Wea. Forecasting*, 19, 970–992, <https://doi.org/10.1175/826.1>.

Shaw, W.J., L.K. Berg, J. Cline, et al., 2019: The Second Wind Forecast Improvement Project (WFIP2): General Overview, *Bull. Amer. Meteor. Soc.*, 100(9), 1687–1699, <https://doi.org/10.1175/BAMS-D-18-0036.1>.

Steenburgh, W.J., C.F. Mass, and S.A. Ferguson, 1997: The Influence of Terrain-Induced Circulations on Wintertime Temperature and Snow Level in the Washington Cascades, *Wea. Forecasting*, 12, 208–227.

Wantz, J.W., and R.E. Sinclair, 1981: Distribution of Extreme Winds in the Bonneville Power Administration Service Area, *J. Appl. Meteor.*, 20, 1400–1411.

Whiteman, C.D., S. Zhong, W.J. Shaw, et al., 2001: Cold Pools in the Columbia Basin. *Wea. Forecasting*, 16, 432–447, [https://doi.org/10.1175/1520-0434\(2001\)016<0432:CPITCB>2.0.CO;2](https://doi.org/10.1175/1520-0434(2001)016<0432:CPITCB>2.0.CO;2).

Wilczak, J.M., M. Stoelinga, L.K. Berg, et al., 2019: The Second Wind Forecast Improvement Project (WFIP2): Observational Field Campaign, *Bull. Amer. Meteor. Soc.*, 100(9), 1701–1723, <https://doi.org/10.1175/BAMS-D-18-0035.1>.

Zhong, S., C.D. Whiteman, X. Bian, et al., 2001: Meteorological Processes Affecting the Evolution of a Wintertime Cold Air Pool in the Columbia Basin, *Mon. Wea. Rev.*, 129, 2600–2613.



## **Environmental Science Division**

Argonne National Laboratory  
9700 South Cass Avenue, Bldg. #240  
Lemont, IL 60439

[www.anl.gov](http://www.anl.gov)



Argonne National Laboratory is a U.S. Department of Energy  
laboratory managed by UChicago Argonne, LLC